



U.S. DEPARTMENT OF
ENERGY

PNNL-19616

Ship Effect Measurement with Fiber Optic Neutron Detectors

Kenneth King and Rashe Dean, Virginia State University

Shahzad Akbar, Virginia State University Faculty

Richard T. Kouzes and Mitchell L. Woodring, PNNL Mentors

July 2010



Pacific Northwest
NATIONAL LABORATORY

*Proudly Operated by **Battelle** Since 1965*

DISCLAIMER

This report was prepared as an account of work sponsored by an agency of the United States Government. Neither the United States Government nor any agency thereof, nor Battelle Memorial Institute, nor any of their employees, makes **any warranty, express or implied, or assumes any legal liability or responsibility for the accuracy, completeness, or usefulness of any information, apparatus, product, or process disclosed, or represents that its use would not infringe privately owned rights.** Reference herein to any specific commercial product, process, or service by trade name, trademark, manufacturer, or otherwise does not necessarily constitute or imply its endorsement, recommendation, or favoring by the United States Government or any agency thereof, or Battelle Memorial Institute. The views and opinions of authors expressed herein do not necessarily state or reflect those of the United States Government or any agency thereof.

PACIFIC NORTHWEST NATIONAL LABORATORY

operated by
BATTELLE

for the
UNITED STATES DEPARTMENT OF ENERGY
under Contract DE-AC05-76RL01830

Printed in the United States of America

Available to DOE and DOE contractors from the
Office of Scientific and Technical Information,
P.O. Box 62, Oak Ridge, TN 37831-0062;
ph: (865) 576-8401
fax: (865) 576-5728
email: reports@adonis.osti.gov

Available to the public from the National Technical Information Service,
U.S. Department of Commerce, 5285 Port Royal Rd., Springfield, VA 22161
ph: (800) 553-6847
fax: (703) 605-6900
email: orders@ntis.fedworld.gov
online ordering: <http://www.ntis.gov/ordering.htm>

ACKNOWLEDGEMENT

This work was supported by the US Department of Energy,
National Science Foundation, and Pacific Northwest National
Laboratory.

Ship Effect Measurements With Fiber Optic Neutron Detector

Kenneth King and Rashe Dean, Virginia State University

Shahzad Akbar, VSU Faculty

Richard Kouzes and Mitchell Woodring, PNNL Mentors

July 2010

Pacific Northwest National Laboratory

Richland, Washington 99352

Summary

The main objectives of this research project was to operate, test and characterize an innovatively designed scintillating fiber optic neutron radiation detector manufactured by Innovative American Technology with possible application to the Department of Homeland Security screening for potential radiological and nuclear threats at US borders (Kouzes 2004). One goal of this project was to make measurements of the neutron ship effect for several materials.

Radiation detectors based on scintillation operate on the principle that energetic particles or gamma rays produce scintillation light when they interact with an inorganic crystalline material such as thallium doped sodium iodide [NaI(Tl)] or an organic plastic such as polyvinyl toluene doped with anthracene (C₁₄H₁₀). The scintillation photons are converted into millions of electrons by a photomultiplier tube whose output can then be further amplified and counted to produce a pulse-height spectrum for analysis of the radiation. The neutron detector tested during the present research is based upon a new design: wavelength shifting plastic fibers surrounded by scintillation material and neutron absorber that generate optical scintillations that are observed by phototubes. Spectral analysis is performed with sophisticated computer software to distinguish neutrons from gamma ray induced signals by comparison of the pulse shape and amplitude.

A particular problem studied was that of cosmic ray neutrons. The details of neutron backgrounds observed in detectors used for non-proliferation monitoring are not well understood. An objective of this project was to gain a better understanding of the origins of neutron backgrounds at the Earth's surface, and to develop methods for distinguishing backgrounds from true source-related events.

The detection of cosmic-ray produced neutrons varies with detector elevation, geomagnetic latitude and materials in the vicinity, e.g., "ship effect" neutrons from large structures. These material related effects, although documented, are difficult to measure because of the low cosmic-ray neutron rates at the surface. They are also important in that they can cause nuisance alarms when screening the transport of massive cargo. Additionally, the relative importance of spallation neutrons caused by cosmic ray hadrons and muons is not well understood. These deficiencies are to be addressed by using the cosmic-ray like neutron energy spectrum from the LANSCE facility at Los Alamos National Laboratory as well as neutrons from "purely" muon induced spallation in the underground facility at Pacific Northwest National Laboratory (PNNL) to form a new understanding of spallation neutron spectra from standardized objects and material.

One significant source of variation in the observed neutron background is caused by the "ship effect," which gives an enhanced production of spallation neutrons from dense, large masses such as a ship and its cargo. The ship effect is particularly striking because of the low neutron background over water. Although the effect is so named because of where it was first observed, large steel masses and other materials in commerce have been observed to cause an increase in the neutron background on land as well [Kouzes 2008a]. Conversely, large concrete structures and overburden can shield background neutrons, while not generating spallation due to the low atomic number of these materials. Even though the natural neutron background is small, its variation can affect the sensitivity of detection systems [Kouzes 2008b].

The results of this work can be applied to active interrogation techniques and to various non-proliferation monitoring systems, including those deployed worldwide by DOE. For example, this work has the potential to reduce the minimum detectable quantity of plutonium whose detection forms a key element in the SNM detection mission. These methods can be applied to both the currently used ^3He -based neutron detectors and the new generation of alternative neutron detectors [Kouzes 2009; Van Ginhoven 2009]. Additionally, this work is expected to assist in the development of new, multiple-channel neutron timing/coincidence instruments, i.e., multiplicity counters, designed to work with the alternative technology neutron detectors. The development of such multiplicity counters and continued development of the measurement techniques would be a logical follow-on to this work.

The Virginia State University DOE FaST/NSF summer student-faculty team made measurements with the fiber optic radiation detector at PNNL above ground to characterize the ship effect from cosmic neutrons, and underground to characterize the muon contribution.

This study found an increase in the ship effect with neutron density, but differences with previous work require further research.

ACRONYMS AND ABBREVIATIONS

cps	counts per second
DOE	U.S. Department of Energy
IAT	Innovative American Technologies
PNNL	Pacific Northwest National Laboratory
PVT	Polyvinyl Toluene (plastic) scintillation gamma detector
RPM	Radiation Portal Monitor
SAIC	Science Applications International Corporation

CONTENTS

Summary	iv
1. Introduction	1
2. Equipment and Detector Calculations	1
2.1. IAT Scintillating Fiber Optic Neutron Radiation Detector	2
2.2. Description of Sources	3
2.3. Detector Solid Angle	3
2.3.1. Solid Angle Calculation	5
2.3.2. Angular Dependency for Solid Angle Calculation	8
2.4. Detector Efficiency Determination with Source	13
2.5. Material	15
3. Poisson Distribution	16
4. Facilities	17
4.1. Description of Building 318	17
4.2. Description of Building 331G	18
4.3. Description 2425 Underground Laboratory	19
5. Data and Analysis	21
5.1. Pb Data	21
5.2. Brass	29
5.3. Tungsten	32
5.4. Steel	34
6. Discussion	35
6.1. Pb Results	35
6.2. Brass Results	36
6.3. Steel Results	37
6.4. Tungsten Results	37
7. Conclusions	39
8. Future Research	40
9. Acknowledgements	40
10. Publications	40
11. APPENDIX: Description of Data Analysis Software	41
11.1. Description of the IAT Sensor Data Capture Software	41
11.2. Operation of the IAT Application SDC	43

11.3. Description of ROOT Software	46
--	----

Figures

Figure 1. IAT detector system.....	2
Figure 2. Locations of Source on IAT Detector	3
Figure 3. Efficiency of Detector.....	4
Figure 4. Solid Angle.....	5
Figure 5. Solid Angle Dimensions.....	6
Figure 6. Source Emission.....	7
Figure 7. Mathematica Program	7
Figure 8. Geometry for Cube	8
Figure 9. Geometry for Cylinder	11
Figure 10. Building 318 Laboratory	17
Figure 11. Indoor Background vs. Poisson	18
Figure 12. 331G Testing Area.....	18
Figure 13. Outside Background vs. Poisson	19
Figure 14. Underground Testing Area	20
Figure 15. Underground Background.....	21
Figure 16. Building 318 Lab Pb Setup	21
Figure 17. Building 318 Lab Plot of Pb cps Versus Distance	23
Figure 18. Building 318 Lab Plot of Poisson versus Pb Multiplicity	24
Figure 19. Building 331G Pb Setup.....	24
Figure 20. Building 331G Pb data for cps and Solid Angle versus Distance	26
Figure 21. Building 331G Plot of Poisson and Multiplicity Data	27
Figure 22. Underground Experimental Setup.....	28
Figure 23. Underground Poisson Distribution and Multiplicity Data.....	29
Figure 24. Building 331G Brass Setup.....	30
Figure 25. Brass CPS Versus Distance	31
Figure 26. 331G Brass Poisson Versus Multichannel	32
Figure 27. Building 331G Tungsten Setup	32
Figure 28. 331G Tungsten Poisson Versus Multichannel.....	33
Figure 29. Building 331G Steel Setup	34
Figure 30. Building 331G Steel Poisson Versus Multichannel Data.....	35

Figure 31. Seven Neutrons From Pb Captured With the OScope Software 36

Figure 32. Neutron Production Rate Versus Materials at 0 cm 37

Figure 33. Plot of Neutron Density Versus 4-Fold Multiplicity (Kouzes et al. 2008)..... 38

Figure 34. Plot of Multiplicity Versus Neutron Density 39

Figure 35. Multichannel View 42

Figure 36. Pulse Height View 43

Figure 37. Pulse Width 43

Figure 38. SDC Select Site View 44

Figure 39. Detector Selection Menu 44

Figure 40. Detector Properties View..... 45

Figure 41. Select Detector View 46

Figure 42. Data Capture Utility..... 46

Figure 43. Starting ROOT Software 47

Figure 44. Changing Directory in ROOT 48

Figure 45. Opening Common Folder in ROOT..... 49

Figure 46. Opening Specific Folder in ROOT 49

Figure 47. Creating n42.list Folder in ROOT program 50

Figure 48. Opening n42.list Folder from ROOT program 50

Figure 49. Saving n42.list in ROOT program 51

Figure 50. Creating Media Directory in ROOT..... 52

Figure 51. Running ROOT program into Excel 52

Figure 52. Opening PeakEasy Folder from Desktop..... 53

Figure 53. Running PeakEasy Software 54

Figure 54. Opening File onto PeakEasy Software 55

Figure 55. Viewing Spectrum onto PeakEasy 56

Figure 56. Saving Spectra as Text File on PeakEasy 57

Tables

Table 1. Sources..... 3

Table 2. Excel Solid Angle for Rectangle 10

Table 3. Excel Solid Angle for Cylinder 12

Table 4. Effective Solid Angle..... 12

Table 5. Detector Efficiency for Source at 0 cm From Detector Enclosure 13

Table 6. Detector Efficiency for Source at 0 cm from Detector Enclosure	13
Table 7. Detector Efficiency for Source at Center from Different Distances	14
Table 8. Detector Efficiency for Source at Center Using Mathematica.....	14
Table 9. Materials used in this study.....	15
Table 10. Indoor Background vs. Poisson	17
Table 11. Outside Background vs. Poisson.....	19
Table 12. Underground Background vs. Poisson.....	20
Table 13. Building 318 Measurement for Pb	22
Table 14. Lead Building 318 Poisson versus Multiplicity Measurement.....	23
Table 15. Building 331G Pb Measurements	25
Table 16. Building 331G Pb Multiplicity Results.....	26
Table 17. Summary of Total Events for Each Facilities	28
Table 18. Underground Measurements Poisson Versus Multichannel	29
Table 19. Pulse Height Brass	30
Table 20. Building 331G Poisson Versus Mutilplicity Events for Brass	31
Table 21. Building 331G Poisson Versus Multichannel Events for Tungsten.....	33
Table 22. Building 331G Poisson Versus Multichannel Events for Steel.....	34
Table 23. Summary of Multiplicity Results.....	38

1. Introduction

National security is one of the major issues in the world. New destructive technologies are constructed every day. One threat is the possibility of radiological or nuclear sources being used as a terrorist weapon; sources of most concern include: complete weapons of mass destruction (WMD); improvised nuclear devices (IND); special nuclear material (SNM) for weapons construction, including plutonium and highly enriched uranium (HEU); and material or assemblies for radiological dispersal devices (RDD), also known as dirty bombs (Kouzes 2005). To prevent these illicit materials from entering the United States, radiation portal monitor (RPM) systems with neutron detectors have been deployed at all US border ports of entry, where these devices scan all vehicles and cargo to identify any significant threats.

Over the last several years, the Department of Homeland Security (DHS) has monitored incoming commerce using radiation portal monitors. A problem has arisen whereby a limited supply of ^3He has eliminated this material from use for neutron detection for portal monitor applications. Therefore, alternative neutron detection technologies are being investigated for use in radiation portal monitor systems (Van Ginhoven 2009). Many different companies have designed alternative neutron detection technologies. One of the newest was manufactured by Innovative American Technologies (IAT), which is a fiber optic based neutron scintillation detector. The main purpose of the research reported here is to measure the ship effect using the IAT “ten by ten inch” neutron detector.

One background to be dealt with in neutron detection is the “ship effect.” The term “ship effect” arose in the 1970s when neutron detectors were used to look for the presence of nuclear weapons on ships at sea (G.W. Phillips 2005). Each day hundred of ships would trigger the alarm of the neutron detectors and after each search no illicit materials were discovered. It was observed that an elevated neutron count rate was present near any large ship, and this was attributed to cosmic-ray-related neutrons produced in the iron of the ships. Ship effect neutrons are produced by the interaction of cosmic-ray-produced secondary neutrons and, to a much lesser degree, muons with material through various nuclear interaction mechanisms (Y.F. Wang 2001).

In this report, the sensitivity of the IAT detector is evaluated in several aspects. Some possible substances in cargo were placed at varying distances from the detector to measure the response. The same method was repeated with sources to test the instrument’s ability to detect harmful material that are shielded. Underground testing of the detector was the last evaluation, to extract data in an environment where there is no penetration of cosmic ray neutrons. The work reported here was to help determine the efficiency of the plastic fiber neutron detector and characterize the ship effect from various materials by analyzing count rate and spectral measurement data.

2. Equipment and Detector Calculations

This section describes the detector, materials and facilities used for the measurements. The detector technology is described and its efficiency is determined. The analysis software and its operation is presented. The materials tested and the facilities used are described.

2.1. IAT Scintillating Fiber Optic Neutron Radiation Detector

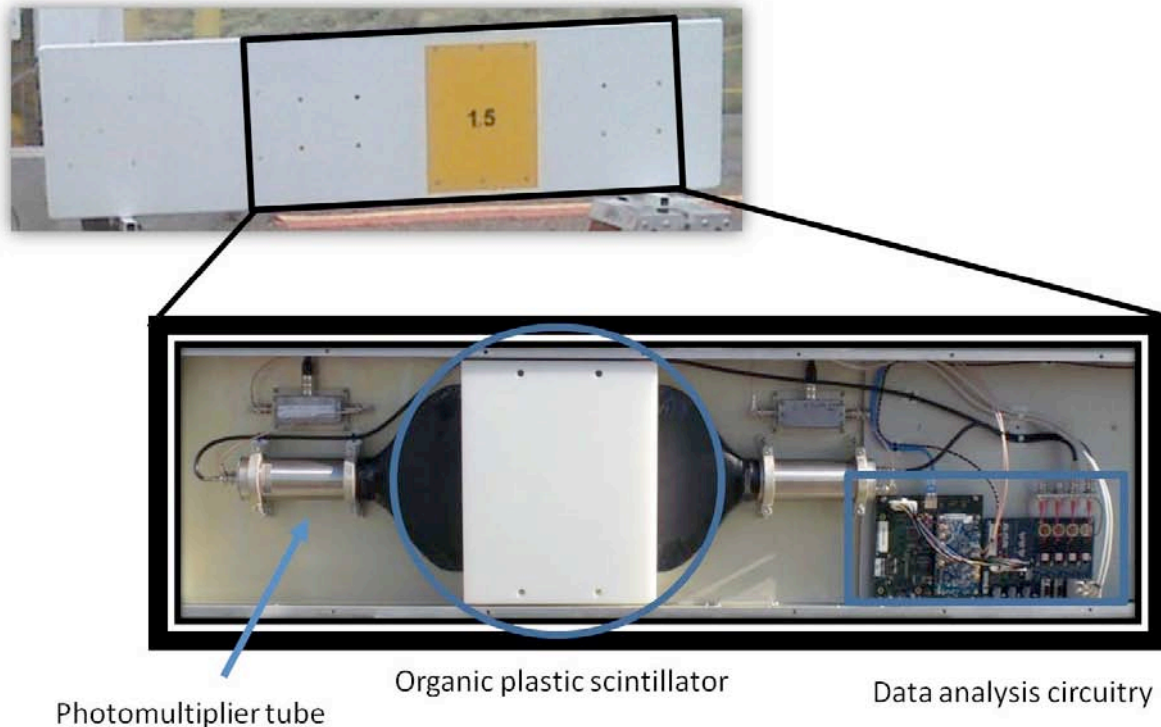


Figure 1. IAT detector system

The IAT neutron detector uses non-scintillating plastic fibers (BC-704 from Saint Gobain) that are coated with ${}^6\text{Li}/\text{ZnS}(\text{Ag})$. The fibers are arranged side-by-side and the detector has four layers of fibers. The active width (coated) of the fiber array is 0.25 m and the active length is 0.25 m. Fibers extend beyond the 0.25 m active length and are bundled at both ends into 0.05-m-diameter photomultiplier tubes. Figure 1 shows the (black) fiber array covered by the polyethylene moderator and the photomultiplier tubes.

The ${}^6\text{Li}/\text{ZnS}(\text{Ag})$ serves as neutron absorber and phosphor. Thermal neutrons interact via the ${}^6\text{Li}(n,\alpha){}^3\text{H}$ reaction, and the resultant charged particles produce light in the zinc sulfide. The plastic wavelength shifting fibers conduct the light to the photomultiplier tubes.

On one side of the fiber array the polyethylene is 0.25 m x 0.25 m x 0.05 m (10 inch x 10 inch x 2 inch) thick and on the other side it is 0.25 m x 0.25 m x 0.38 m (1.5 inch) thick. Separate tests were conducted with a neutron source facing each of the polyethylene sides, as well as tests with the 0.05-m-thick polyethylene removed and thinner sheets substituted.

2.2. Description of Sources

The neutron source used for these tests was ^{252}Cf , with a half-life of 2.645 years. The source was purchased from Isotope Products Laboratory (IPL) and given a PNNL ID of 60208-44. The source was measured by IPL to be $21.91 \pm 1.25 \mu\text{Ci}$ on October 1, 2009.

Source Name	Date of Use	Activity (μCi)	Activity (ng)	Neutron Emission Rate
Californium-252 Source	6/22/10	18.2	33.6	77 280
Californium-252 Source (Bare)	7/6/10	18.0	33.3	76 590

Table 1. Sources

Two configurations of the neutron sources were used in measuring the efficiency of the IAT detector. On June 22nd, the source inside a moderating pig was used at distances ranging from zero to one meter. The same source was used on July 6th, but it was removed from the pig. This bare source was attached to the outside of the detector with tape at five different points in the area of the scintillator, center, top right, top left, bottom right and bottom left (Shown in Figure 2). Then the source was moved back ten inches and the same procedure was repeated.

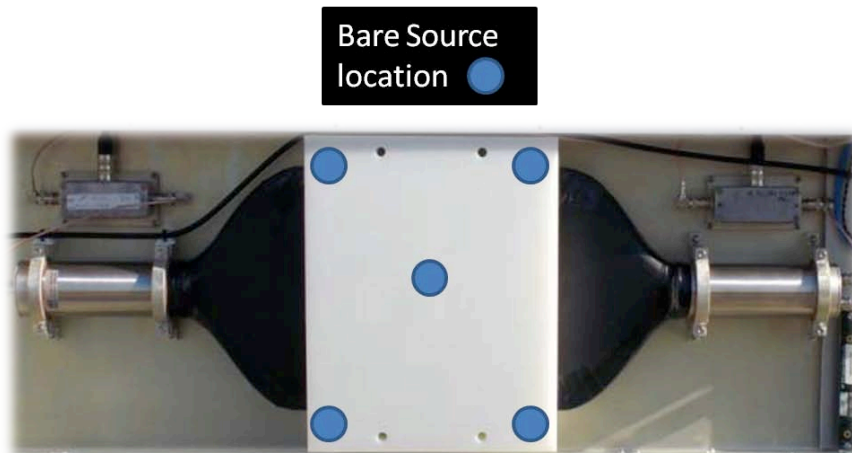


Figure 2. Locations of Source on IAT Detector

2.3. Detector Solid Angle

Understanding the efficiency of the IAT detector is one of the main aspects of this research. It was necessary to have a precise figure for the detector efficiency in order to relate the number of pulses counted to the number of neutrons or photons incident on the detector (Knoll p116). The efficiency that is required is the intrinsic efficiency, which is the probability of detecting a neutron if it hits the area of the detector. This is in contrast to the absolute efficiency, which is the probability of detecting a neutron emitted at some specific point in space.

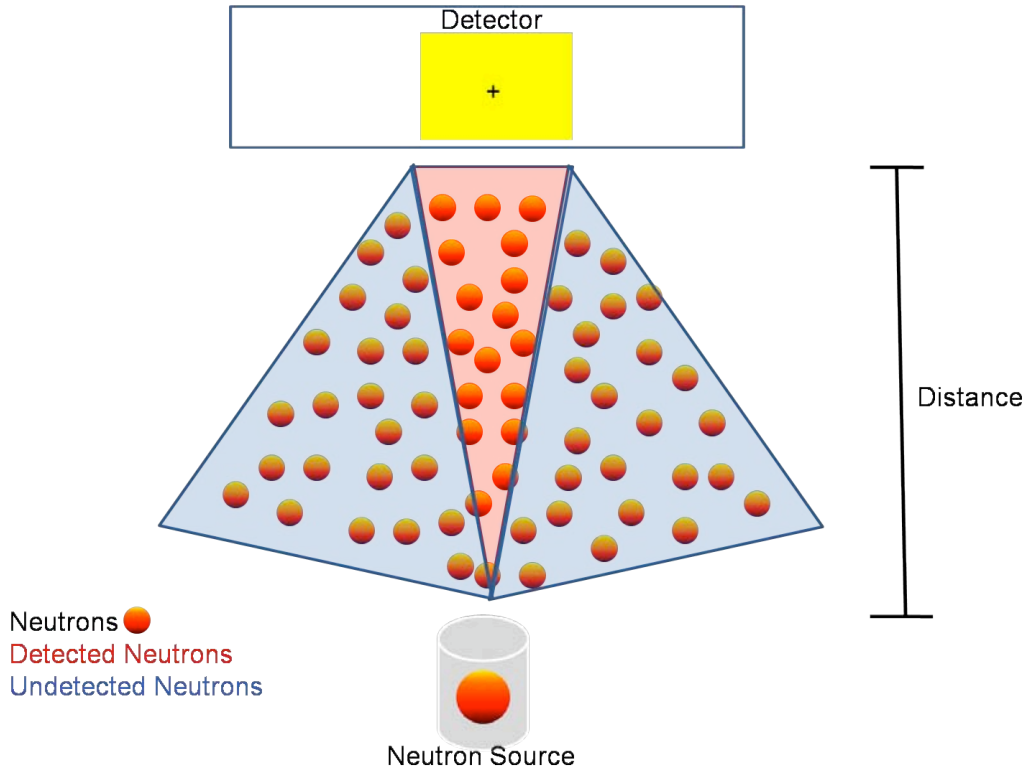


Figure 3. Efficiency of Detector

The intrinsic efficiency does not include the solid angle subtended by the detector as an implicit factor (Knoll p117). The equation is:

$$\text{Intrinsic efficiency } (\epsilon_I) = (\text{number of pulses recorded}) / (\text{Number of radiation quanta incident on detector})$$

$$\text{Absolute efficiency } (\epsilon_A) = (\text{number of pulses recorded}) / (\text{Number of radiation quanta emitted by source})$$

The number of pulses recorded is the net counts or net count rate, which is the measured count rate minus the background count rate.

$$\text{Net count rate} = \text{Rate of pulses recorded (counts per second)} - \text{Background count rate}$$

The number of radiation quanta incident on the detector (net incident rate) can be calculated for any given source that is used in an experiment by including a correction for geometry. The neutron sources used have a known mass in nanograms (ng). This can be used to give the number of neutrons emitted per second by multiplying by 2300 cps/ng.

2.3.1. Solid Angle Calculation

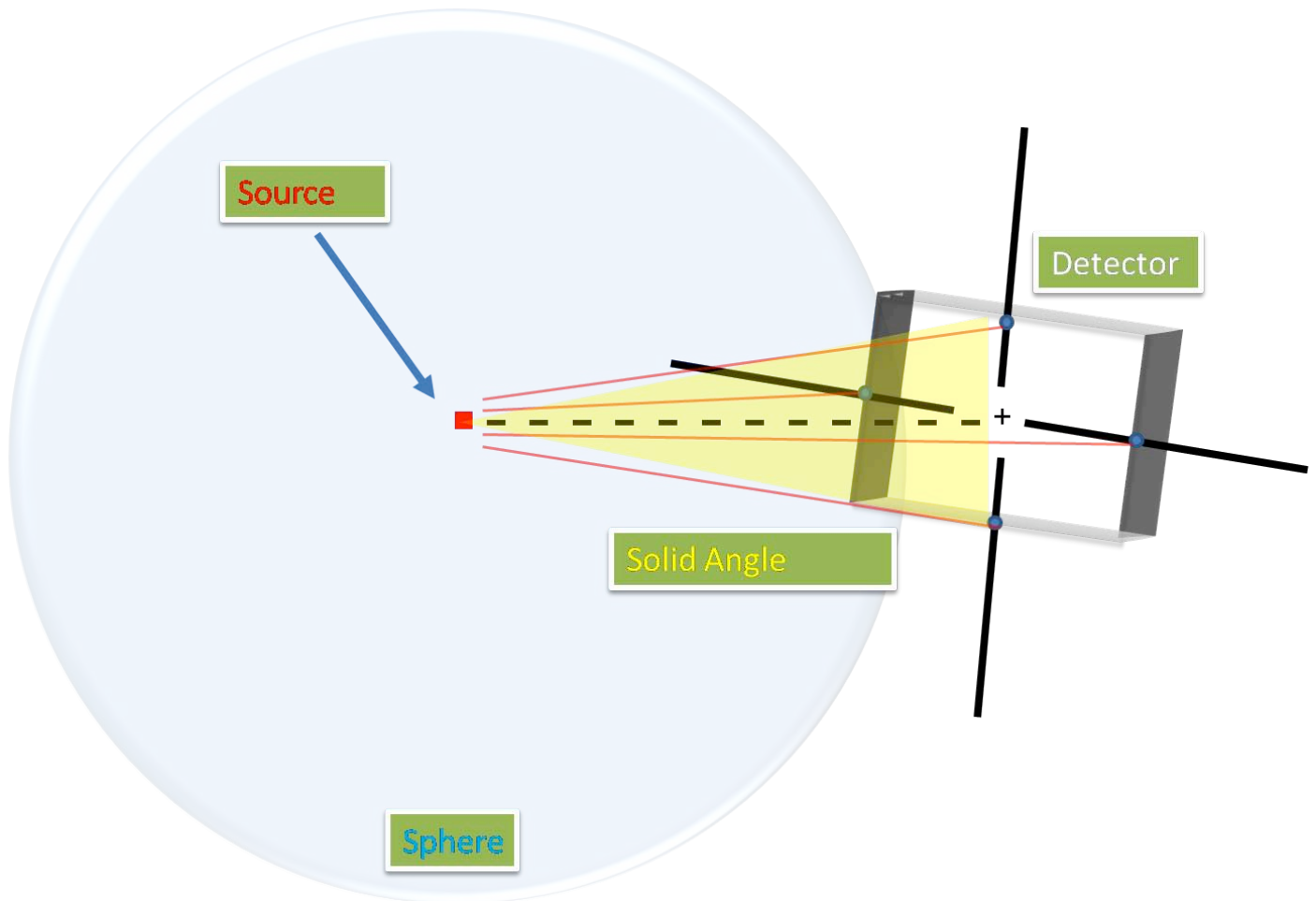


Figure 4. Solid Angle

The solid angle is an essential factor needed for a calculation of the efficiency of any detector. This factor is defined by an integral over the detector surface that faces the source (Knoll p118). The surface area of a sphere has a solid angle of 4π steradian.

The integral of this surface area of the sphere is computed by using two orthogonal angles, phi and theta.

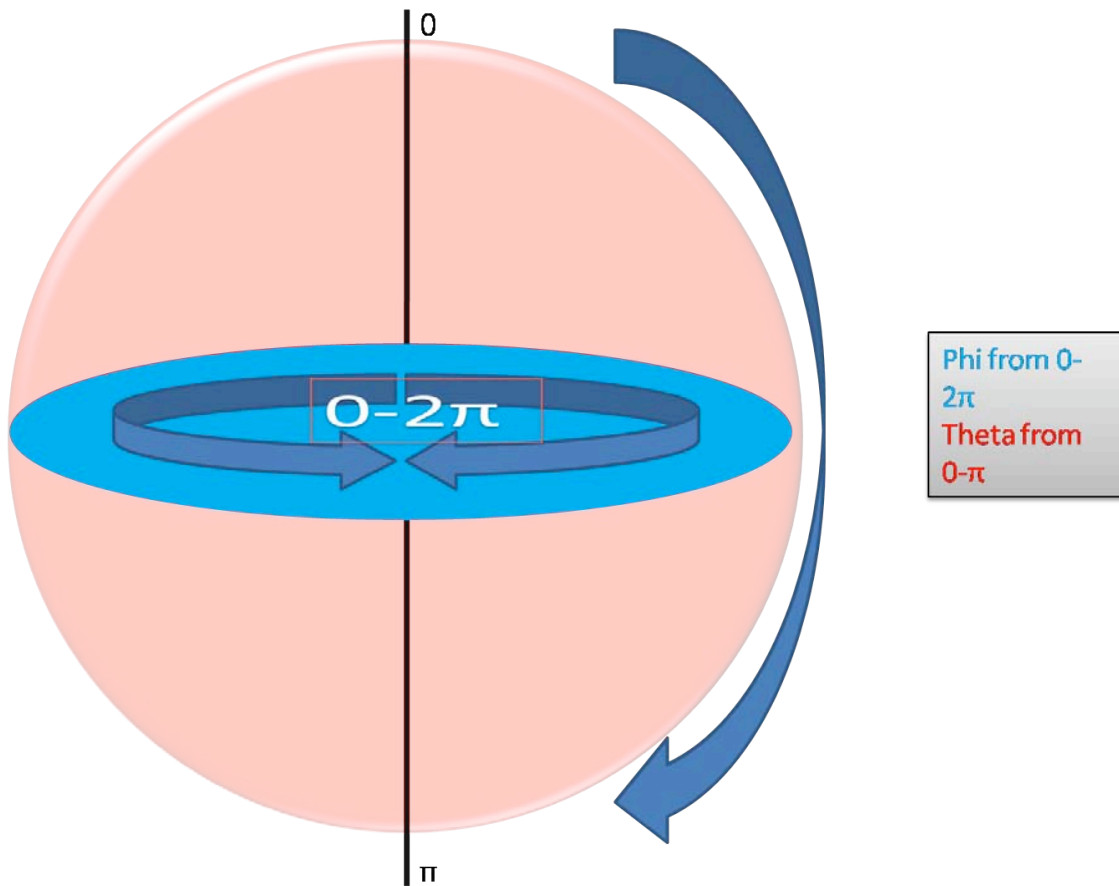


Figure 5. Solid Angle Dimensions

As show in Figure 5, Phi describes the rotation angle around the sphere axis in the horizontal plane and ranges from 0 to 2π ; Theta describes the angle relative to the rotation axis and ranges from 0 to π .

The integral of this sphere is represented by:

$$\int_0^{2\pi} d\phi \int_0^{\pi} \sin\theta d\theta$$

$$2\pi \times 2 = 4\pi$$

As seen in Figure 6, the detector only “sees” fewer than half of the neutrons emitted by the source due to the geometry.

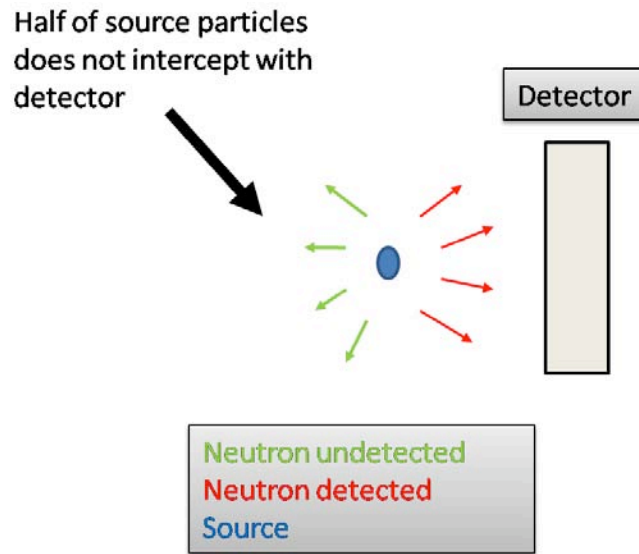


Figure 6. Source Emission

All aspects are taken into consideration, and the solid angle calculation is derived and executed using the program Mathematica.

Wolfram Mathematica 7.0 - [cartesian solid angle.nb]

File Edit Insert Format Cell Graphics Evaluation Palettes Window Help

cartesian solid angle.nb

```
xmax = 19.25
ymax = 61
z = 7.975
N[Integrate[4 z (x^2 + y^2 + z^2)^(-3/2), {x, 0, xmax}, {y, 0, ymax}]]
```

19.25
61
7.975
4.63258

Solid angle equation for point source

Solid angle

Xmax= width of detector
Ymax= height of detector
Z= distance of source from detector

Figure 7. Mathematica Program

Mathematica was used to compute the solid angle with respect to distance, but we did not implement the computation of angular dependency, so an Excel spread sheet was used to accomplish that goal for shapes such as a cube and cylinders.

2.3.2. Angular Dependency for Solid Angle Calculation

a. Solid Angle for a Cube

For some measurements, a cubic geometry of material was used. If N_I particles are incident upon an target with N_T nuclei per unit are, the number of detected particles N_D is given by the equation (Cook 1980).

$$N_D = N_I N_T \int \int d\sigma/d\Omega \, d\Omega$$

where Ω is the solid angle and $d\sigma/d\Omega$ is the differential scattering cross-section expressed by

$$d\sigma/d\Omega = \frac{ND}{N_I N_T \Omega}$$

The solid angle subtended by a rectangle of width $2w$ and length $2h$ at a point $P(x_p, y_p, z_p)$ may be calculated using an exact analytical solution (Gotoh & Yagi 1971).

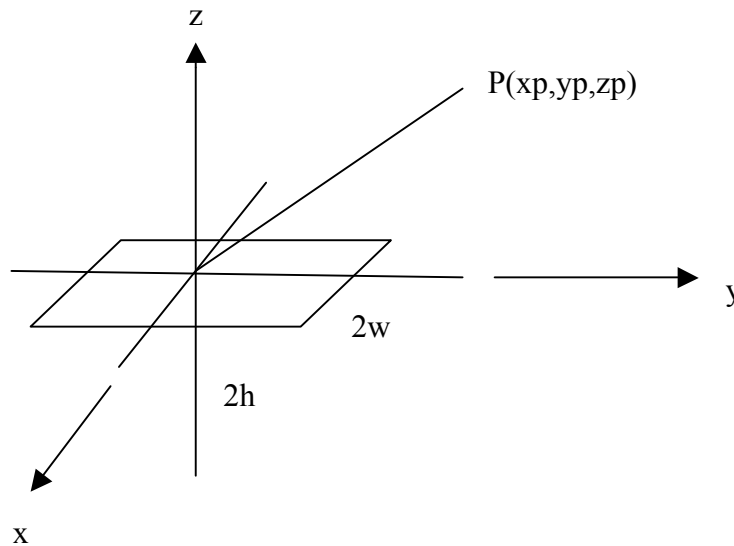


Figure 8. Geometry for Cube

The solid angle subtended by the rectangle at the point P is given by the integral:

$$\Omega = h \int dx \int \frac{dy}{(x^2 + y^2 + z^2)^{1/2}}$$

The analytical solution to this double integral is exactly expressed by a sum of inverse trigonometric functions:

$$\begin{aligned} \Omega(x_p, y_p, z_p) &= \arctan \frac{(w + x_p)(h + y_p)}{z_p[(w + x_p)^2 + (h + y_p)^2 + z_p^2]^{1/2}} \\ &+ \arctan \frac{(w + x_p)(h - y_p)}{z_p[(w + x_p)^2 + (h - y_p)^2 + z_p^2]^{1/2}} \\ &+ \arctan \frac{(w - x_p)(h + y_p)}{z_p[(w - x_p)^2 + (h + y_p)^2 + z_p^2]^{1/2}} \\ &+ \arctan \frac{(w - x_p)(h - y_p)}{z_p[(w - x_p)^2 + (h - y_p)^2 + z_p^2]^{1/2}} \end{aligned}$$

Using this equation in Excel, the solid angle for the center position of the point P, located directly 207 cm above the center of the rectangle was calculated as follows:

Solid angle subtended by a rectangle to a point above its center

width of the rectangle	w	12.7	width 2w	25.4	
length of the rectangle	h	12.7	length 2h	25.4	
x-coordinate of the point	x _p	0			
y-coordinate of the point	y _p	0			
z-coordinate of the point	z _p	207	height	200	thickness 7

	xp1	12.7	$w + xp$
	yp1	12.7	$h + yp$
	yp2	12.7	$h - yp$
	xp2	12.7	$w - xp$
	n1	161.29	$xp1 * yp1$
	d1	207.7777	$(xp1^2 + yp1^2 + zp^2)^{0.5}$
	d2	43009.99	$d1 * zp$
	t1	0.00375	$n1/d2$
first factor	ang1	0.00375	$\arctan(t1)$
	n2	161.29	$xp1 * yp2$
	d3	207.7777	$(xp1^2 + yp2^2 + zp^2)^{0.5}$
	d4	43009.99	$d3 * zp$
	t2	0.00375	$n2/d4$
second factor	ang2	0.00375	$\arctan(t2)$
	n3	161.29	$xp2 * yp1$
	d5	207.7777	$(xp2^2 + yp1^2 + zp^2)^{0.5}$
	d6	43009.99	$d5 * ZP$
	t3	0.00375	$n3/d6$
third factor	ang3	0.00375	$\arctan(t3)$
	n4	161.29	$xp2 * yp2$
	d7	207.7777	$(xp2^2 + yp2^2 + zp^2)^{0.5}$
	d8	43009.99	$d7 * zp$
	t4	0.00375	$n4/d8$
fourth factor	ang4	0.00375	$\arctan(t4)$
solid angle	sol	0.015	$ang1 + ang2 + ang3 + ang4$
	$4\pi/sol$	837.8574	$4\pi/sol$
	$sol/4\pi$	0.001194	$sol/4\pi$

Table 2. Excel Solid Angle for Rectangle

The result for this geometry at a point from a rectangular detector plane was that the subtended solid angle was $\Omega = 0.015$ steradians. Similar calculations were performed for the various geometries encountered in the experiments using the IAT rectangular detector.

b. Solid Angle for a Cylinder

For some measurements, a cylindrical geometry of material was used. The case of a solid angle subtended by a cylinder was approximated by an analytical solution (Guest 1961).

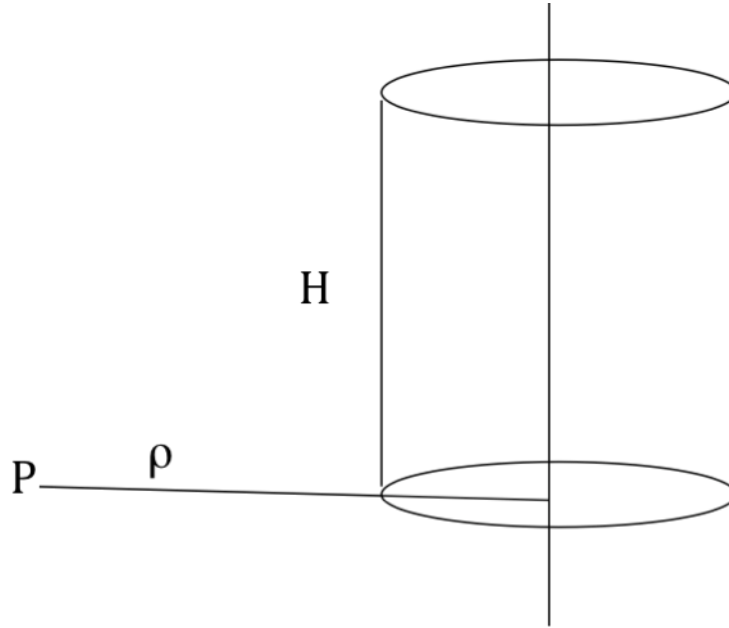


Figure 9. Geometry for Cylinder

The solid angle subtended at the point P in the base plane from the axis of a right circular cylinder of unit radius and height H is expressed by the integral:

$$\Omega = 2H \int (H^2 + S^2)^{-1/2} d\phi$$

where $S = \rho \cos\phi - (1 - \rho^2 \sin^2\phi)^{1/2}$

The approximate analytical solution for the solid angle is given by:

$$\Omega = \frac{2H(1 + 1/6\rho^2)}{\rho [H^2 + (\rho - \pi/4 - 1/5\rho)^2]^{1/2}}$$

The solid angle for the case of a cylinder was calculated using the above formula in Excel for a cylinder of radius $r1$ and height $H1$ at a point at a distance $x1$ from the cylinder axis.

solid angle subtended by a right circular cylinder to a point

Radius of the cylinder	r1	36	cm
Height of the cylinder	H1	53.5	cm
Distance between the point and the cylinder axis	x1	100	cm
	r	1	
	2H	1.486111	
	H	0.743056	
	x	2.777778	
	n1	1.486111	2H
	n2	1.0216	$1 + 1/6x^2$
	n3	1.518211	$n1 * n2$
	a	0.8575	$\pi/4 + 1/5x$
	x-a	1.920278	$x - a$
	d1	3.687467	$(x - a)^2$
	d2	2.059028	$(H^2 + d1)^{0.5}$
	d3	5.719524	$x(d2)$
Solid Angle	sol	0.265444	$n3/d3$
	W	0.530887	$2(sol)$

Table 3. Excel Solid Angle for Cylinder

The solid angle subtended by the cylinder for this particular geometry was calculated as 0.2654 steradians. These calculations were performed for the various geometries in the experiments.

c. Solid Angle for Actual Geometry

Using Mathematic, it is possible to find the effective solid angle of each distributed geometry, i.e., the average of the solid angle over each point in the volume.

Material	Effective Solid Angle (From Mathematica)
Fe	0.822
Brass	0.537
W	1.835
Pb	0.956

Table 4. Effective Solid Angle

2.4. Detector Efficiency Determination with Source

Tables 5 and 6 show a calculation of the efficiency with respect to x, y, and z. In the tables, z is the distance between the IAT detector and the source, while x and y are the horizontal and vertical placement of the source, respectively. These two tables were calculated using the function generated in the Excel program created specifically for calculating the solid angle of the source. The intrinsic efficiency is found from the calculated solid angle, the net counts per second and the source emission rate (76 590 neutrons/s) as follow:

$$\epsilon_i = (\text{Neutron Detected} / \text{Neutron Emitted}) * (4\pi / \text{Solid Angle})$$

The scintillator is set back about 7 cm from the front outside of the detector enclosure.

Position	X (cm)	Y (cm)	Z (cm)	Background (cps)	Source (cps)	Net (cps)	Calculated solid angle	Intrinsic efficiency
center	0	0	7	2	6689.8	6687.8	3.50	0.31
top right	12.7	12.7	7	2	2105	2103	1.19	0.29
top left	-12.7	12.7	7	2	2212.3	2210.3	1.19	0.30
bottom right	12.7	-12.7	7	2	1690.2	1688.2	1.19	0.23
bottom left	-12.7	-12.7	7	2	2076	2074	1.19	0.28

Table 5. Detector Efficiency for Source at 0 cm From Detector Enclosure

Table 5 shows the calculations for solving the ϵ_i (Intrinsic Efficiency) using a point source 7 cm away from the detector (0 cm from face of detector + 7 cm from center of detector). We measured the point source at five different locations on the detector (center, top right, top left, bottom right, and bottom left). There was one discrepancy in the acquired information showing a huge drop in counts per second (cps) when taken at the bottom right. To get the average ϵ_i , we discarded the ϵ_i at this location and simply added the rest together and divided by four (number of locations). The average ϵ_i the detector gave off in this case came to 0.295 or 29.5%.

Position	X(cm)	Y(cm)	Z(cm)	background	Source (cps)	Net (cps)	Calculated solid angle	Intrinsic efficiency
center	0	0	32.4	2	990.7	988.7	0.534315	0.30
top right	12.7	12.7	32.4	2	710.2	708.2	0.390492	0.29
top left	-12.7	12.7	32.4	2	737.4	735.4	0.390492	0.31
bottom right	12.7	-12.7	32.4	2	715.7	713.7	0.390492	0.30
bottom left	-12.7	-12.7	32.4	2	680.4	678.4	0.390492	0.285

Table 6. Detector Efficiency for Source at 0 cm from Detector Enclosure

Table 6 shows the calculations for solving the ϵ_I (Intrinsic Efficiency) using a point source 32.4 cm away from the detector (25.4 cm [10 inches] from face of detector + 7 cm from center of detector). The dimension of 10 inches was chosen to match the size of the Pb cube. We measured the point source at five different locations on the detector (center, top right, top left, bottom right, and bottom left). Throughout the process of calculating the ϵ_I , we found the values to be close to each other. To get the average ϵ_I , we added together each E_I that we found and divided the total number by five (number of locations). The average ϵ_I the detector provided in this case came to 0.298 or 29.8%.

Position	X(cm)	Y(cm)	Z(cm)	background	Source (cps)	Net (cps)	Calculated solid angle	Intrinsic efficiency
center	0	0	7	2	6689.8	6687.8	3.50	0.31
center	0	0	32.4	2	990.7	988.7	0.53	0.30
center	0	0	107	2	107	105	0.056	0.31
center	0	0	207	2	36	34	0.015	0.37

Table 7. Detector Efficiency for Source at Center from Different Distances

Table 7 shows measured rates and computed solid angle using Excel. Table 8 shows the outcome when calculating the efficiency using Mathematica instead of Excel.

Position	X(cm)	Y(cm)	Z (cm)	Background (cps)	Source (cps)	Net (cps)	Mathematica solid angle	Intrinsic efficiency
center	0	0	7	1.33	6690	6688.67	3.50	0.31
center	0	0	32.4	1.33	991	989.67	0.53	0.30
center	0	0	107	1.33	107	105.67	0.056	0.31
center	0	0	207	1.33	36	34.67	0.015	0.37



Table 8. Detector Efficiency for Source at Center Using Mathematica



The data given from Tables 7 and 8 illustrate that Excel and Mathematica calculation agree for the solid angle and intrinsic efficiency, thus verifying that the formulas used in each of these programs are consistent.

2.5. Material

Measurements of the Ship Effect are a significant part of this research. Our goal is to use different materials to measure interactions with cosmic rays using the IAT neutron detector.

Table 9. Materials used in this study

Material	Information on materials	Description and Dimension of shape	Image
Lead (Pb)	Atomic number: 82 Atomic weight: 207.2 Description: soft heavy toxic malleable metallic element Density: 11.3 g/cm ³ Mass: 320 kg	Shape: cube Substance: sealed bricks Height: 30.5 cm Width: 30.5 cm Length: 30.5 cm	
Brass (Cu + Zn)	Atomic number(Cu): 29 Atomic weight(Cu): 63.1 Atomic number(Zn): 30 Atomic weight(Zn): 65.38 Average Atomic number (Brass 70Cu/30Zn)= 29.3 Average Atomic weight (Brass 70Cu/30Zn)= 64.1 Description: an alloy of copper (~70%) and zinc (~30%) Density: 8.74 g/cm ³ Mass: 307 kg	Shape: cylinder Substance: four large rings, four small rings and two small cylinder Height: 53.3 cm Width: 36 cm	

<p>Tungsten(W)</p>	<p>Atomic number: 74 Atomic weight: 183.84 Description: gray to white metallic element extracted from wolframite, scheelite, and other minerals Density: 16.2 g/cm³ Mass: 52 kg</p>	<p>Shape: cylinder and rectangle Substance: four half circle thick plates and one rectangle block Height: 21.59 cm Width: 15.24 cm Length: 15.24 cm</p>	
<p>Iron (Fe)</p>	<p>Atomic number: 26 Atomic weight: 55.845 Description: A silvery-white, lustrous, and malleable metallic element Density: 6.1 g/cm³ Mass: 91 kg</p>	<p>Shape: cube Substance: large amount of 1 inch nuts</p>	

3. Poisson Distribution

The purpose of Poisson distribution is to produce a probability of the number of times a certain event occurs within a given time period. The Poisson distribution only works under the circumstances that the user has a known average rate and if the events are independent of one another.

$$P(k) = \frac{\bar{x}^k e^{-\bar{x}}}{k!}$$

\bar{x} = known average of a distribution

$P(x)$ = probability that there are k occurrences

e = base of natural logarithm

$k!$ = factorial of k, the number of occurrences of an event

The result of the equation with a k of three would give the user

$$\frac{\bar{x}^3}{6e^{\bar{x}}}$$

If \bar{x} were 0.5, P(x) would be 0.0126.

While radioactive decay follows a Poisson distribution, the ship effect does not since the multiple neutrons emitted simultaneously in a spallation event are correlated.

4. Facilities

4.1. Description of Building 318

Building 318 is located in the 300 areas of the PNNL facilities. The building was used to measure different materials in an indoor environment to test the ship effect. Figure 10 shows measurements being made in the laboratory.

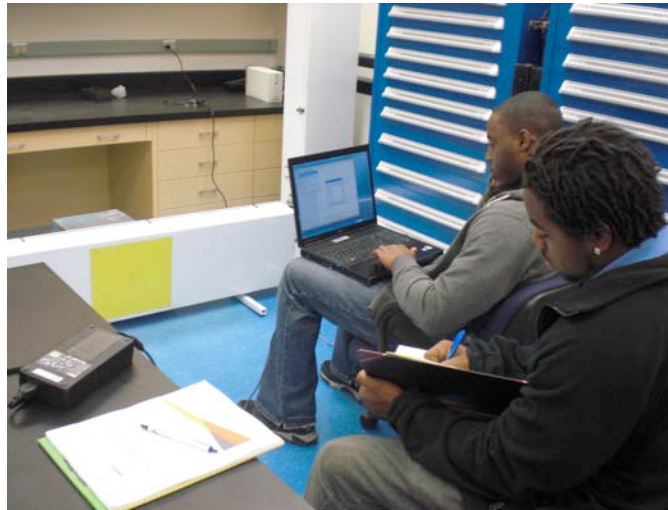


Figure 10. Building 318 Laboratory

Table 10 gives the data for background measured in building 318. Figure 11 shows that the background follows a Poisson distribution to the level of statistics obtained in the measurement.

Table 10. Indoor Background vs. Poisson

Event	total zeroes	total ones	total twos	total threes	total fours	total fives	total sixes	total sevens	total eights
Total	21756	2627	181	12	0	0	0	0	0
%	0.89	0.11	0.0074	0.00049	0	0	0	0	0
Poisson	0.88	0.11	0.0067	0.00028	8.45E-6	2.082E-7	4.27E-9	7.51E-11	1.16E-12

The sum of the total number of counts was 2810 (24 576 including zeros). The Mean for the Poisson distribution is 0.123.

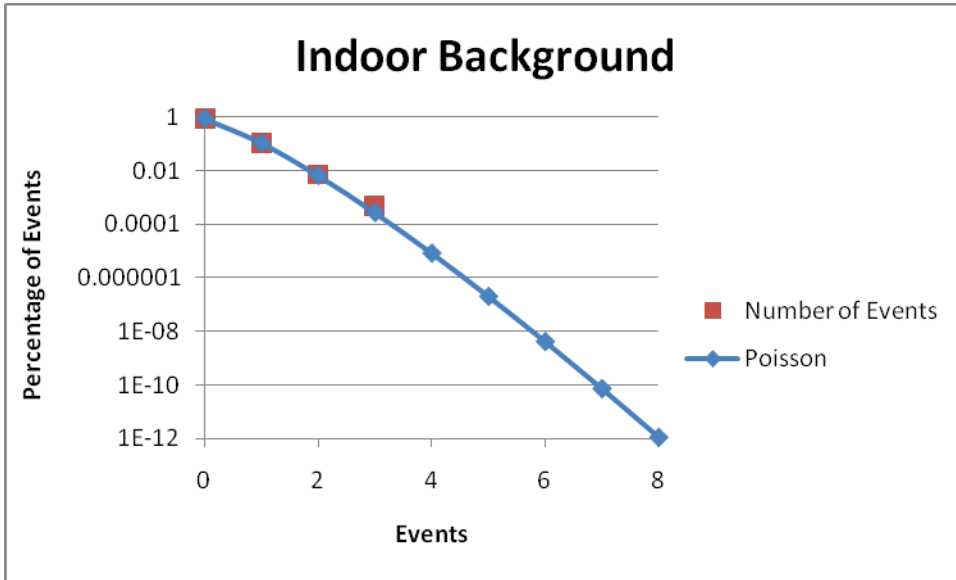


Figure 11. Indoor Background vs. Poisson

4.2. Description of Building 331G

Building 331G is an outdoor site where the RPM (Radiological Portal Monitors) are located and tested. This outdoor site was used to eliminate interference from any radiation source.

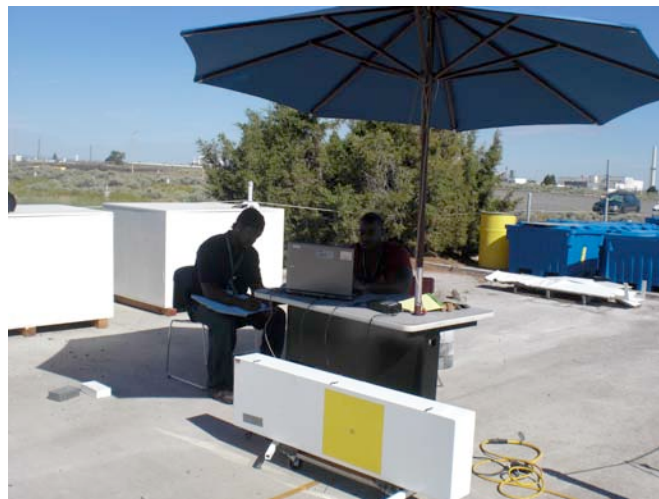


Figure 12. 331G Testing Area

Table 11 shows the background data obtained outside at Building 331G. Figure 13 shows that the background follows a Poisson distribution to the level of statistics obtained in the measurement.

Table 11. Outside Background vs. Poisson

Event	total zeroes	total ones	total twos	total threes	total fours	total fives	total sixes	total sevens	total eights
Total	68670	4865	191	2	0	0	0	0	0
%	0.93	0.066	0.0026	2.71E-5	0	0	0	0	0
Poisson	0.93	0.066	0.0024	5.61E-5	1.0E-6	1.42E-8	1.61E-10	1.72E-12	1.53E-14

The sum of the total number of counts was 5059 (73 728 including zeros). The Mean for the Poisson distribution is 0.0712.

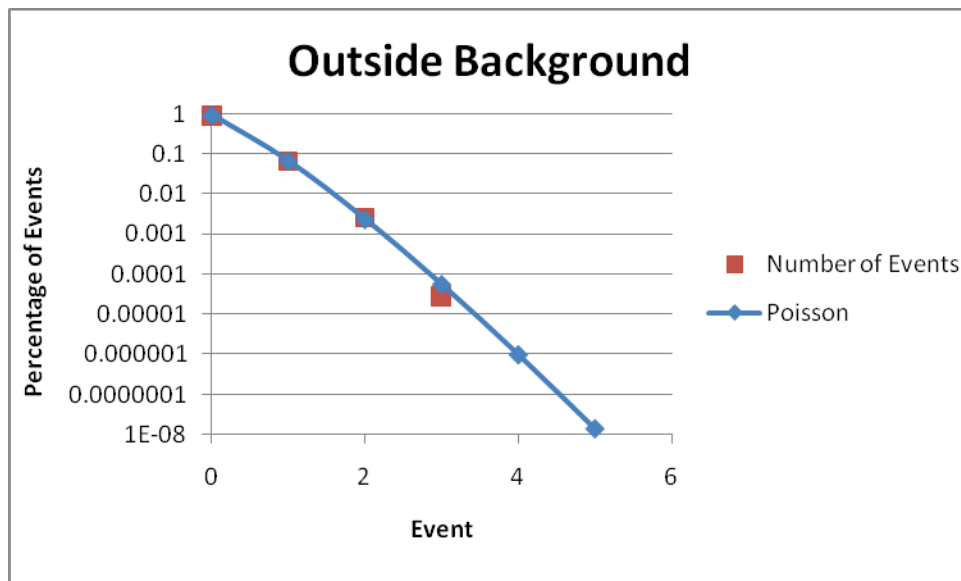


Figure 13. Outside Background vs. Poisson

4.3. Description 2425 Underground Laboratory

The Underground Lab is a special facility at PNNL built to provide a very low background radiation environment. It is built at a depth of 12.2 m (40 feet), which reduces the cosmic ray background significantly (about a factor of 9 in muon rate). Ship effect measurements for a 30.5 cm (12 inch) Pb cube were conducted with the IAT detector in Underground Lab. Figure 14 shows the layout of the underground space.

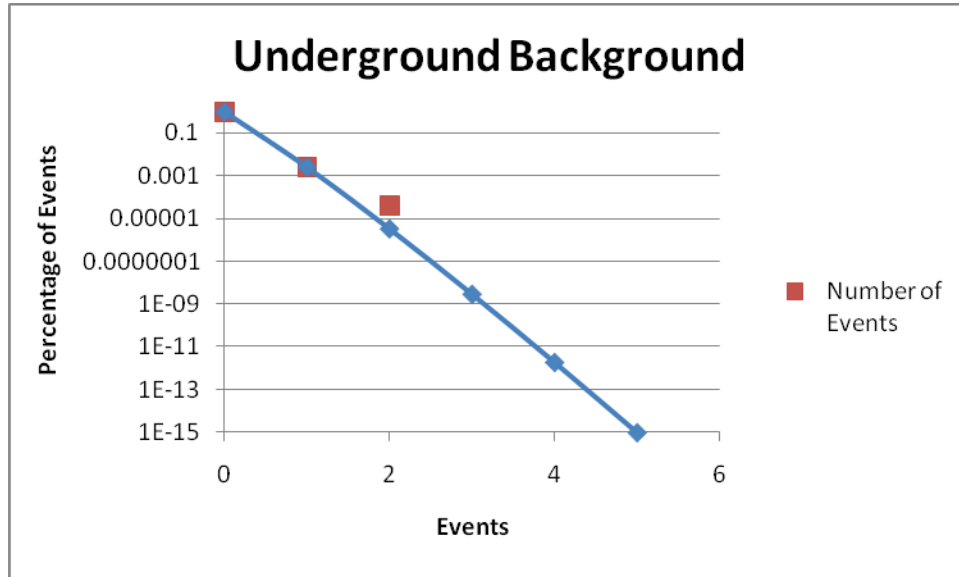


Figure 15. Underground Background

5. Data and Analysis

5.1. Pb Data

i. Pb Data From 318

The setup for Pb inside at 318 is seen in Figure 16.



Figure 16. Building 318 Lab Pb Setup

A lead cube was assembled with the dimension of 30.5 cm x 30.5 cm (12"x12"). Table 13 provides the data measured for Pb in Building 318. One background measurement was used for all other measurements, which is a limitation to the results.

Table 13. Building 318 Measurement for Pb

Distance (cm)	Det1 (cps)	Det2 (cps)	Det Sum (cps)	Background	Sum Net cps	Standard Deviation Value	Standard Deviation as %	Excel Solid Angle
0	1.95	1.46	3.41	2.11	1.3	0.068	5%	3.5
10	1.92	1.48	3.39	2.11	1.28	0.068	5%	1.5
20	1.84	1.42	3.26	2.11	1.15	0.067	6%	.73
30	1.88	1.42	3.3	2.11	1.19	0.067	6%	.42
40	1.87	1.4	3.27	2.11	1.16	0.067	6%	.27
50	1.81	1.34	3.16	2.11	1.05	0.066	6%	.24
60	1.85	1.42	3.27	2.11	1.16	0.067	6%	.14
70	1.9	1.39	3.29	2.11	1.18	0.067	6%	.11
80	1.91	1.36	3.27	2.11	1.16	0.067	6%	.083
90	1.85	1.34	3.19	2.11	1.08	0.066	6%	.067
100	1.86	1.34	3.2	2.11	1.09	0.067	6%	.055
150	1.77	1.26	3.03	2.11	0.92	0.065	7%	.026
200	1.58	1.13	2.72	2.11	0.61	0.063	10%	.016

The IAT detector measured the Pb cube in pulse height at distances ranging from zero to two meters. The table above shows the computed information measured by the detector. The excel equation for solid angle of a rectangle was used to calculation the solid angle for each Pb geometry.

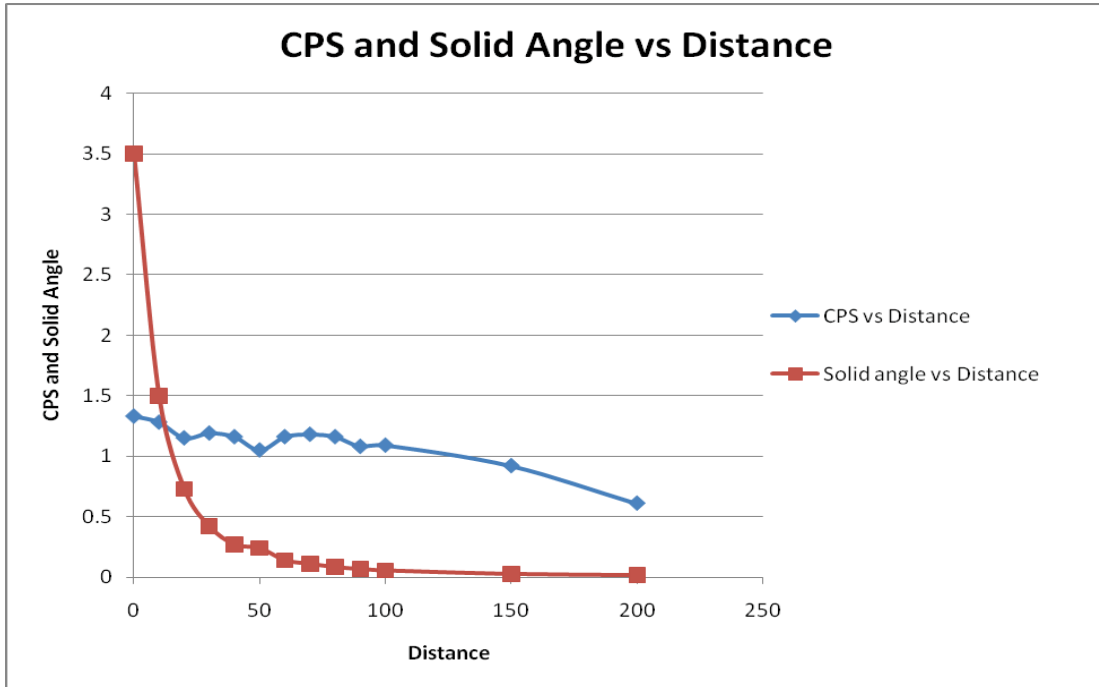


Figure 17. Building 318 Lab Plot of Pb cps Versus Distance

The plotted line of cps versus distance in Figure 17 (blue) illustrates that as distance decreases the detector counted fewer neutrons from the lead cube. The excel solid angle is also shown. It would have been expected that the data curve would follow the solid angle curve, but they deviate greatly. This seems to indicate that the data are contaminated by background in the building that may be changing with time and do not represent a good measurement of the neutron emission rate from spallation events in the lead.

Table 14. Lead Building 318 Poisson versus Multiplicity Measurement

Event	total zeros	total ones	total twos	total threes	total fours	total fives	total sixes	total sevens	total eights
Total	20719	3390	383	47	10	2	1	0	0
%	0.84	0.14	0.016	0.0019	0.000407	8.15E-05	4.07E-05	0	0
Poisson	0.84	0.15	0.013	0.00078	3.45E-05	1.22E-06	3.61E-08	9.15E-10	2.03E-11

Table 14 shows the results from the multiplicity measurement of the Pb in Building 318. The detector was positioned against the lead cube. The measurement time was 40 minutes. The first row gives the number of events seen with the indicated multiplicity in a times window of 100 seconds (0.1 s per channel). The row labeled Percentage was derived from each individual event total divided by sum of all the combined events (example: sum = 24 552; to get percentage for total zeroes, divide total zeroes by sum 20 719 / 24 552 = 0.84). The row labeled Poisson is the

Excel Poisson function result. The Mean used in the function was derived by multiplying each number of events by the event total, after adding them all up, divide by the total number of counts (example: $(0 \cdot 20\,719 + 1 \cdot 3\,390 + 2 \cdot 383 + \dots + 7 \cdot 0 + 8 \cdot 0) / 24\,552$); this number (0.18) is the mean for the Poisson probability.

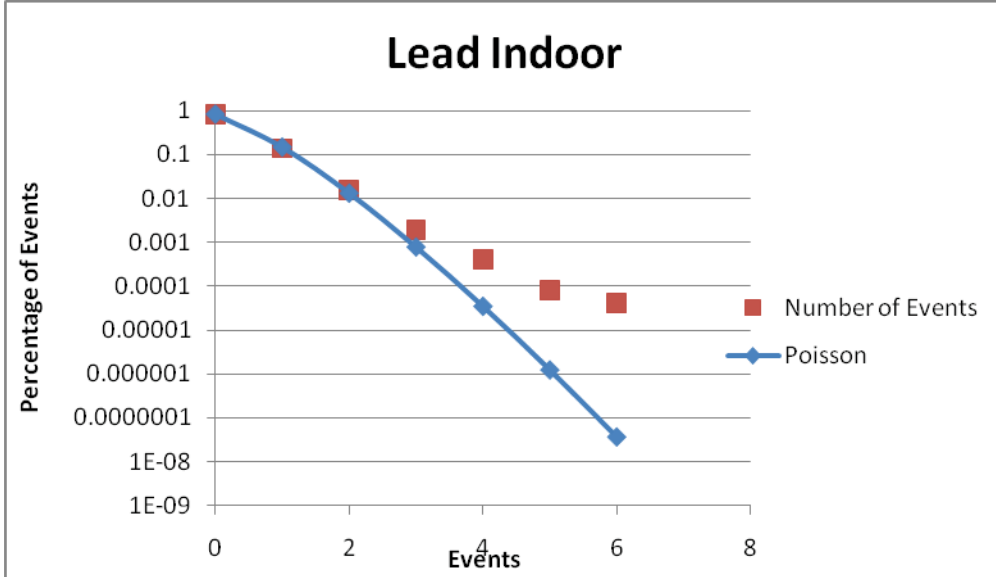


Figure 18. Building 318 Lab Plot of Poisson versus Pb Multiplicity

Figure 18 and Table 14 show the probability of an event occurring. It shows the Poisson Probability Distribution versus the results given from the multiplicity data. The probability is shown in terms of percentage.

ii. Data from 331G for Pb

The setup for Pb Outside at 331G is seen in Figure 41.

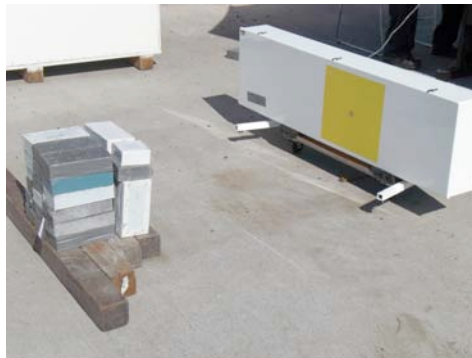


Figure 19. Building 331G Pb Setup

Table 15. Building 331G Pb Measurements

Distance (cm)	Det1 (cps)	Det2 (cps)	Sum (cps)	Net (cps)	Standard Deviation	Standard Deviation Percent	Solid Angle
0	1.38	1.02	2.4	0.98	0.056	6%	3.5
10	1.1	0.93	2.03	0.61	0.054	9%	1.5
20	0.93	0.77	1.7	0.28	0.051	18%	.73
30	0.82	0.91	1.73	0.31	0.051	17%	.42
40	0.84	0.72	1.56	0.14	0.050	36%	.27
50	0.72	0.75	1.47	0.05	0.049	98%	.24
60	0.73	0.74	1.47	0.05	0.049	98%	.14
70	0.85	0.8	1.65	0.23	0.051	22%	.11
80	0.78	0.71	1.49	0.07	0.049	70%	.083
90	0.76	0.73	1.49	0.07	0.049	70%	.067
100	0.65	0.75	1.4	-0.02	0.048	-242%	.055
150	0.69	0.7	1.39	-0.03	0.048	-161%	.026
200	0.72	0.68	1.4	-0.02	0.048	-242%	.016

The IAT detector measured the Pb cube in pulse height mode at distances ranging from zero to two meters. Table 15 shows the information measured by the detector at the 331G outdoor facility. The values beyond 50 cm are all consistent with no signal with the given standard deviation. The excel equation for the solid angle of a rectangle was used to calculation the solid angle.

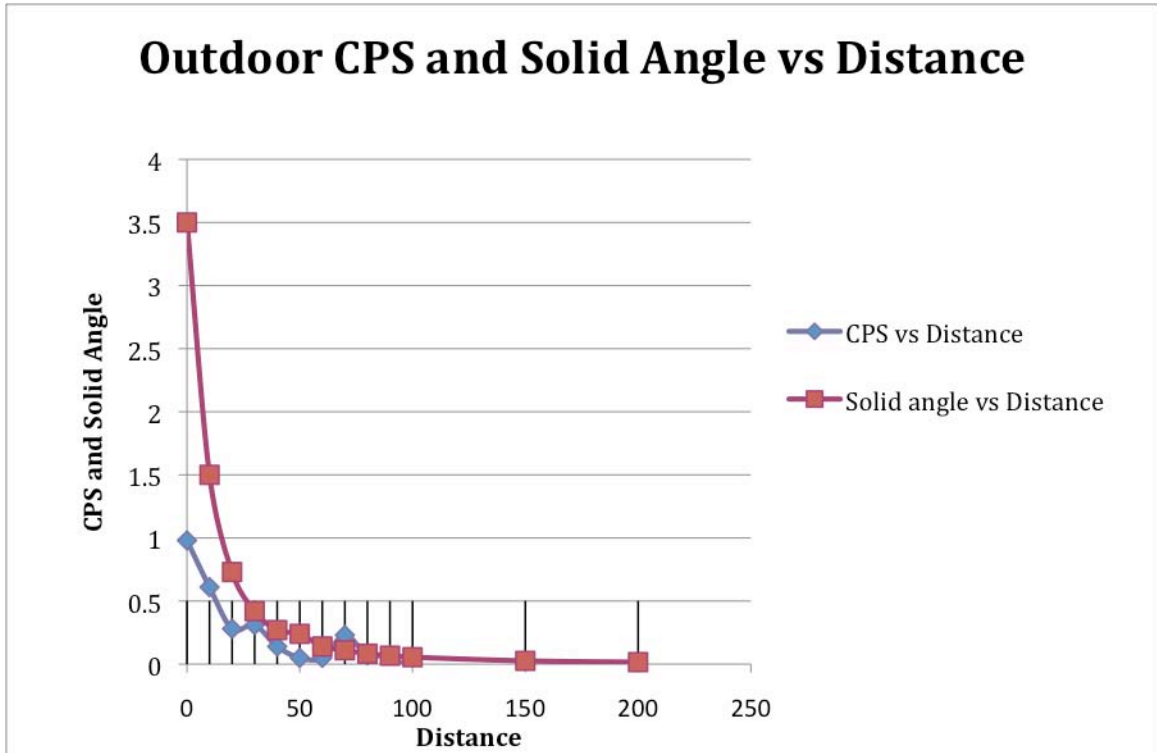


Figure 20. Building 331G Pb data for cps and Solid Angle versus Distance

The plot in Figure 20 illustrates that distance versus cps decreases and levels out in this outdoor environment. The plotted line of cps versus distance (blue) is similar to the indoor plot where there is a trend to fewer counts at larger distance, but not a good correlation with the solid angle.

Table 16. Building 331G Pb Multiplicity Results

Event	total zeroes	total ones	total twos	total threes	total fours	total fives	total sixes	total sevens	total eights
Total	77648	7439	729	83	22	8	1	1	0
%	0.90	0.086	0.0085	0.00097	0.000256	9.31E-05	1.16E-05	1.16E-05	0
Poisson	0.90	0.097	0.0052	0.00019	5.1E-06	1.1E-07	1.99E-09	3.07E-11	4.14E-13

The sum of the total number of counts was 8283 (85 931 including zeros). The Mean for the Poisson distribution is 0.108.

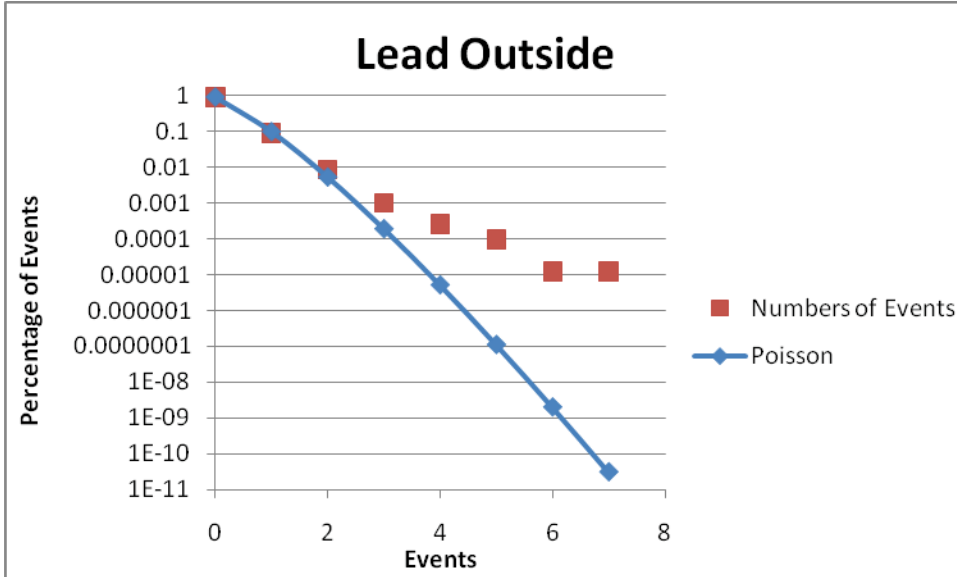


Figure 21. Building 331G Plot of Poisson and Multiplicity Data

Figure 21 and Table 16 show the Poisson distribution and the measurement results given from the multichannel data. The probability is given in terms of percentage. The outdoor measurement of event numbers were similar to the indoor measurement, but the outdoor data had a slightly higher event rate.

iii. Data for Pb from Underground 2425

The setup for Pb underground is seen in Figure 22.

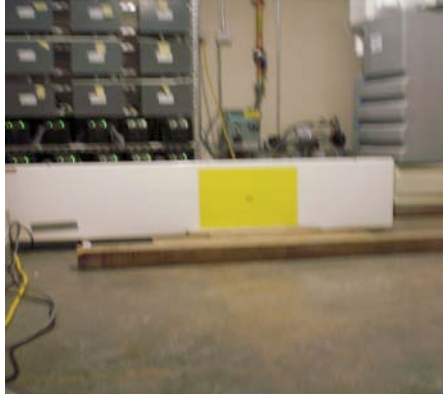


Figure 22. Underground Experimental Setup

Table 17. Summary of Total Events for Each Facilities

Facilities	Back-grnd	total zeroes	total ones	total twos	total threes	total fours	total fives	total sixes	total sevens	total eights	Total 2s-8s	time (min)	rate (cps)
Indoor (318)	2.11	20719	3390	383	47	10	2	1	0	0	443	20	0.369
Outside (331G)	1.42	77648	7439	729	83	22	8	1	1	0	844	70	0.201
Undergrnd (2425)	.06	73469	251	6	1	1	0	0	0	0	8	60	0.0022

Table 17 demonstrates how the multiplicity events ranging from zero to eight varies in different environments. Time played a factor of how many counts exceeding four that were captured. According to Table 17, the count rate was highest inside Building 318. The rate of events underground was only 4% of that above ground. The events underground are presumably from neutrons coming from the walls of the facility. The rate of events of multiplicity 4 and above was 0.0108 cps (13/1200), 0.0076 cps (32/4200), and 0.0003 cps (1/3600) for the indoor, outdoor and underground measurement, respectively. The ratio of the underground to outdoor measurement for events with multiplicity of two to eight in 0.1 second time bins is only 1%. This, combined with a measurement of the muon rate reduction of about nine from above ground (measured by Juniata College students in the summer of 2009) to underground in this facility puts a limit on the muon production of ship effect neutrons of about <10%. It is believed that the muons only produce a few percent at most of the ship effect neutrons. Further measurements will be required to obtain a better limit on this rate

Table 18. Underground Measurements Poisson Versus Multichannel

Event	total zeroes	total ones	total twos	total threes	total fours	total fives	total sixes	total sevens	total eights
Total	73469	251	6	1	1	0	0	0	0
%	0.9965	0.00340	8.14E-5	1.36E-5	1.36E-5	0	0	0	0
Poisson	0.9963	0.00364	6.68E-6	8.16E-9	7.47E-12	5.47E-15	0	0	0

The sum of the total number of counts was 259 (73 728 including zeros). The Mean for the Poisson distribution is 0.0037.

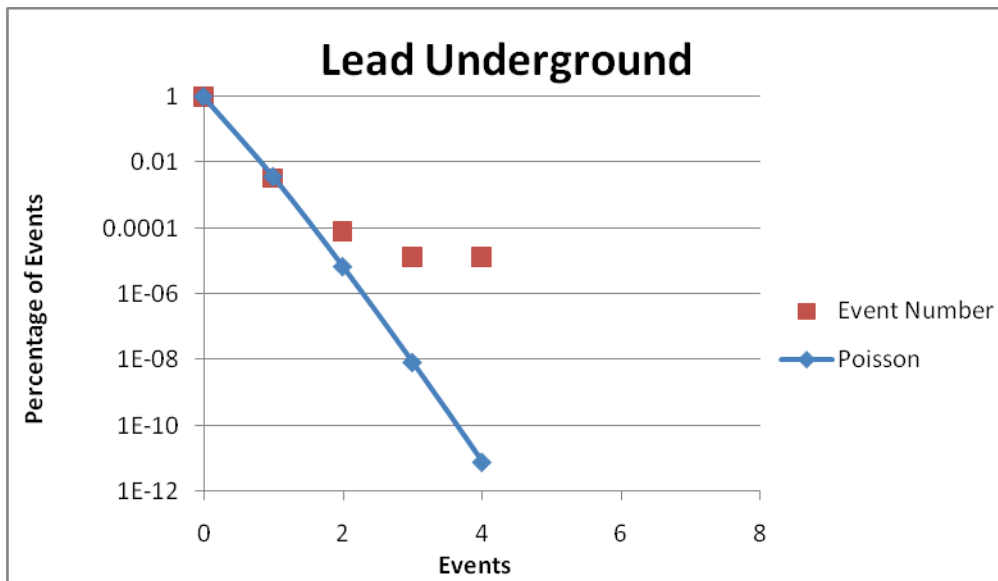


Figure 23. Underground Poisson Distribution and Multiplicity Data

Figure 23 and Table 18 show the probability of an event occurring. They show the Poisson distribution and the measurement results given from the multichannel data. The probability is given in terms of percentage.

5.2. Brass

The setup for brass at 331G is shown in Figure 24.



Figure 24. Building 331G Brass Setup

Table 19. Pulse Height Brass

Det1 (cps)	Det2 (cps)	Sum (cps)	Distance (cm)	counts per second	Standard deviation	% error	Solid Angle
0.88	0.82	1.7	0	0.27	0.051	19%	0.430
0.83	.77	1.6	10	.17	0.050	30%	0.085
0.78	0.75	1.53	20	0.1	0.050	50%	0.034
0.76	0.74	1.5	30	0.07	0.049	71%	0.018
0.74	0.74	1.48	40	0.05	0.049	98%	0.011
0.81	0.76	1.57	50	0.14	0.050	36%	0.008
0.83	0.77	1.6	60	0.17	0.050	30%	0.005
0.81	0.72	1.53	70	0.10	0.050	50%	0.004
0.76	0.68	1.44	80	0.01	0.049	489%	0.003
0.76	0.61	1.37	90	-0.06	0.048	-81%	0.002
0.73	0.76	1.49	100	0.06	0.049	82%	0.002

Table 19 illustrates the efficiency of the detector when it comes to measuring a brass cylinder versus distance. As the results show, some measurements came out to be below the initial background. The solid angle was computed using the excel cylinder calculations.

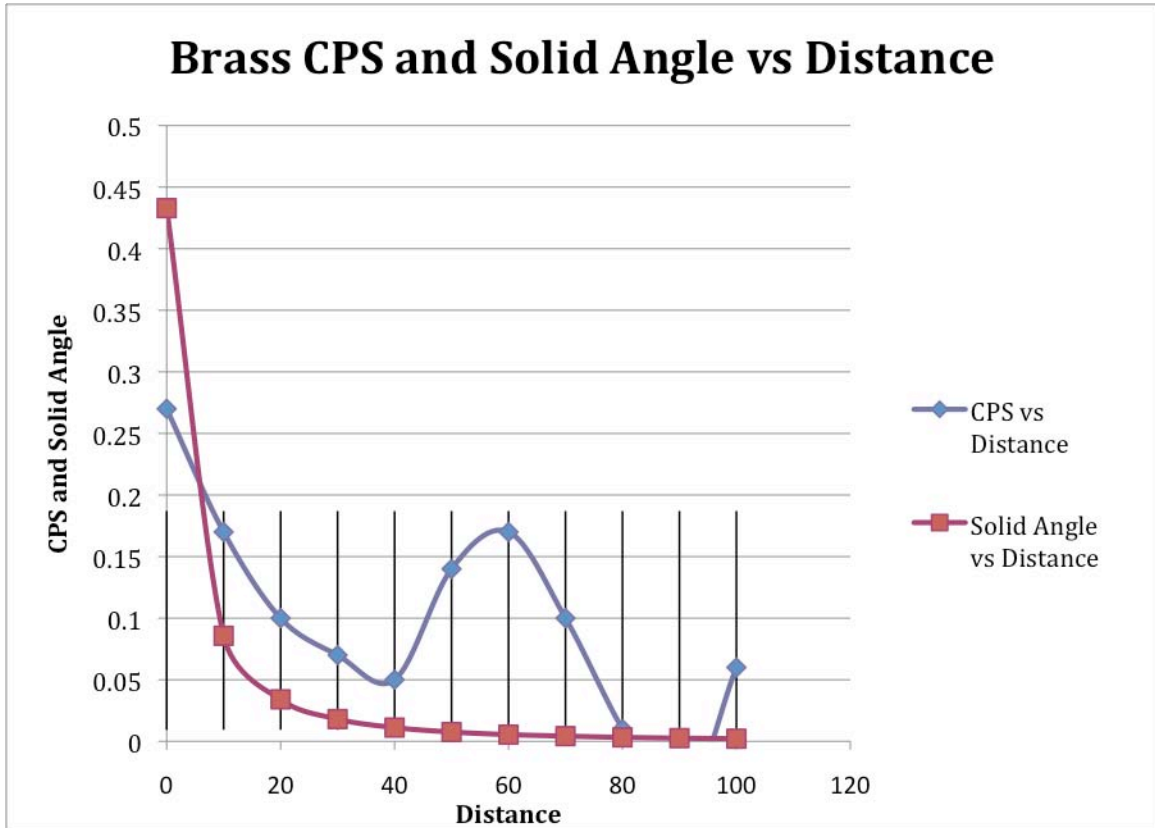


Figure 25. Brass CPS Versus Distance

Figure 25 illustrates that cps (blue) data versus distance fluctuate in the outdoor 331G environment. The solid angle versus distance plot (red) compares the excel calculation to $1/r^2$ distribution. The curve of the solid angle decreases and levels out as distance increases, in exception to the slope

Table 20 shows the Poisson versus multichannel data.

Table 20. Building 331G Poisson Versus Multiplicity Events for Brass

Event	total zeroes	total ones	total twos	total threes	total fours	total fives	total sixes	total sevens	total eights
Total	67796	5546	293	18	1	1	1	0	0
%	0.92	0.075	0.0040	0.00024	1.36E-05	1.36E-05	1.36E-05	0	0
Poisson	0.92	0.077	0.0033	9.14E-05	1.92E-06	3.24E-08	4.55E-10	5.5E-12	5.8E-14

The sum of the total number of counts was 5860 (73 656 including zeros). The Mean for the Poisson distribution is 0.084.

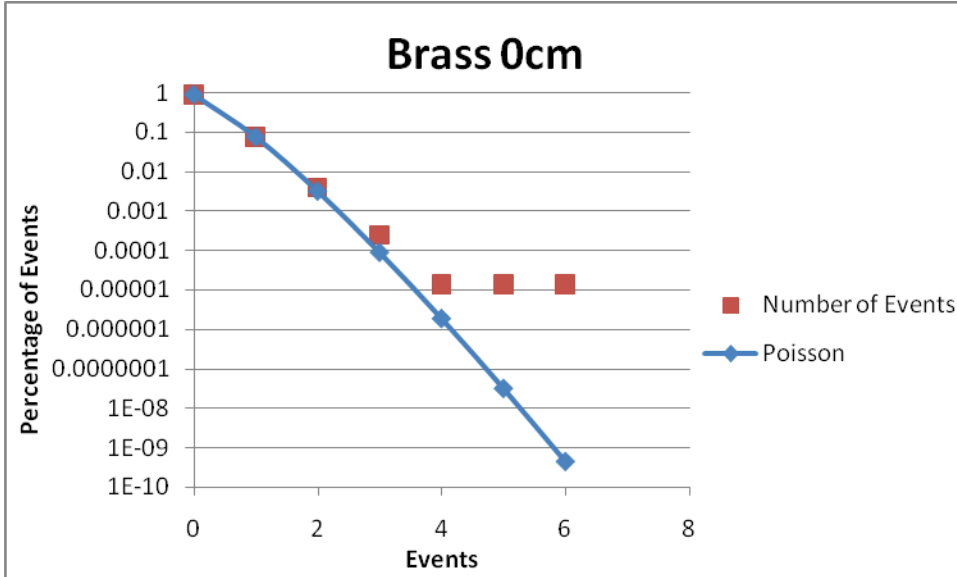


Figure 26. 331G Brass Poisson Versus Multichannel

Figure 26 and Table 20 indicate the probability of an event occurring. They show the Poisson Probability distribution and the measurement results given from the multichannel data.

5.3. Tungsten

The setup for tungsten at 331G is shown in Figure 27.



Figure 27. Building 331G Tungsten Setup

Table 21 shows the multiplicity events for Tungsten.

Table 21. Building 331G Poisson Versus Multichannel Events for Tungsten

Event	total zeroes	total ones	total twos	total threes	total fours	total fives	total sixes	total sevens	total eights
Total	68157	5161	306	23	6	2	0	1	0
%	0.93	0.070	0.0042	0.00031	8.15E-05	2.72E-05	0	1.36E-05	0
Poisson	0.92	0.074	0.0029	7.84E-05	1.57E-06	2.5E-08	3.33E-10	3.8E-12	3.79E-14

The sum of the total number of counts was 5499 (73 656 including zeros). The Mean for the Poisson distribution is 0.0799.

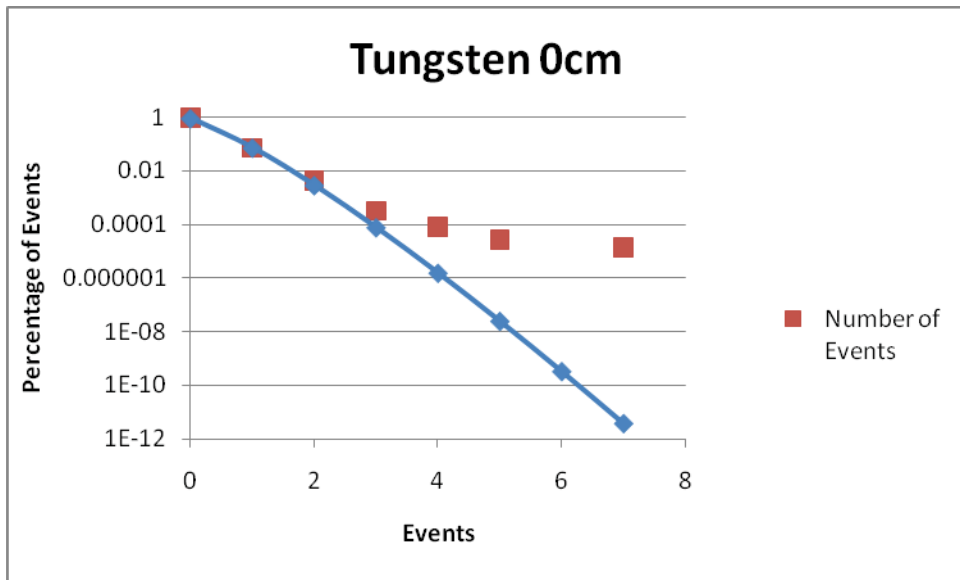


Figure 28. 331G Tungsten Poisson Versus Multichannel

Figure 28 and Table 21 show the probability of an event occurring. They show the Poisson distribution and the measurement results given from the multichannel data. The probability is given in terms of percentage. The tungsten shows the ship effect occurs.

5.4. Steel

Figure 29 shows the setup for steel. The steel was in the form of nuts, so it had a low average density.



Figure 29. Building 331G Steel Setup

Table 22 shows the multiplicity events for Steel.

Table 22. Building 331G Poisson Versus Multichannel Events for Steel

Event	total zeroes	total ones	total twos	total threes	total fours	total fives	total sixes	total sevens	total eights
Total	68375	5062	215	4	0	0	0	0	0
%	0.93	0.069	0.0029	5.43E-05	0	0	0	0	0
Poisson	0.93	0.069	0.0026	6.45E-05	1.21E-06	1.8E-08	2.24E-10	2.4E-12	2.24E-14

The sum of the total number of counts for steel was 5281 (73 656 including zeros). The Mean for the Poisson distribution is 0.0747.

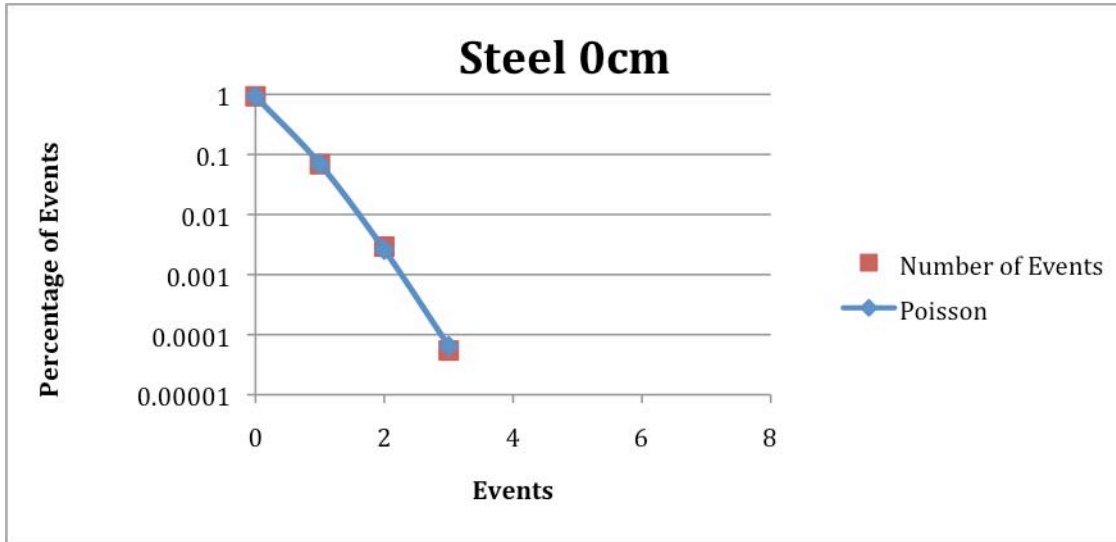


Figure 30. Building 331G Steel Poisson Versus Multichannel Data

Figure 30 and Table 22 give the probability of an event occurring. They show the Poisson distribution versus the actual results given from the multichannel data. The probability is given in terms of percentage. In this case of steel, the data matched that of the Poisson distribution.

6. Discussion

This research consists of using different materials that varied in neutron density to investigate the ship effect. Cosmic ray induced neutrons from any large mass of material do not fit a Poisson distribution due to deviations in the high neutron multiplicity caused by ship effect bursts. The four materials were evaluated to produce results to compared with neutron density.

6.1. Pb Results

The data produce by the Pb cube with the IAT neutron detector confirmed that Pb interaction with cosmic rays created the second highest multiplicity compared to the other three materials. The Pb cube was examined at three different locations with various backgrounds. Table 9 can be used to compare Pb with the other material result in Tables 14, 15, 16. Figure 31 shows an image where seven neutrons in 33 μ s were detected by the IAT during an indoor lab measurement.

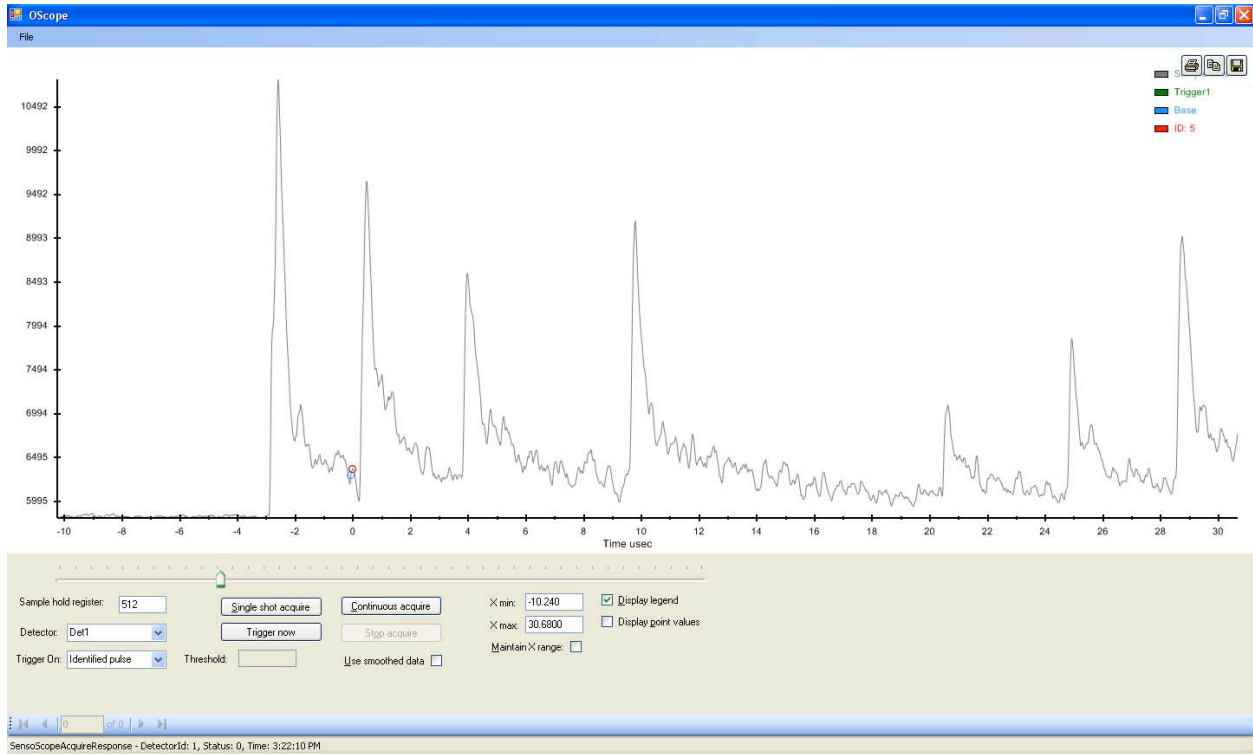


Figure 31. Seven Neutrons From Pb Captured With the OScope Software

6.2. Brass Results

The stack of brass rings gave the second highest neutron count rate in the IAT detector when compared to Pb, steel, and tungsten. When measured by the multiplicity with events having four or more counts per time interval, the brass was the second lowest material with only three counts exceeding four events per interval. There were times where, as we moved the detector farther away from the brass material, the acquired counts per second were lower than that of the initially measured background. Since brass is the next to lowest neutron density material of the four, the results met the expectations of the research.

The density of brass corresponded with its multiplicity count rate compared to the other three materials. Brass emitted more neutrons, as shown in Figure 32, but overall emitted fewer counts over a multiplicity rate of four.

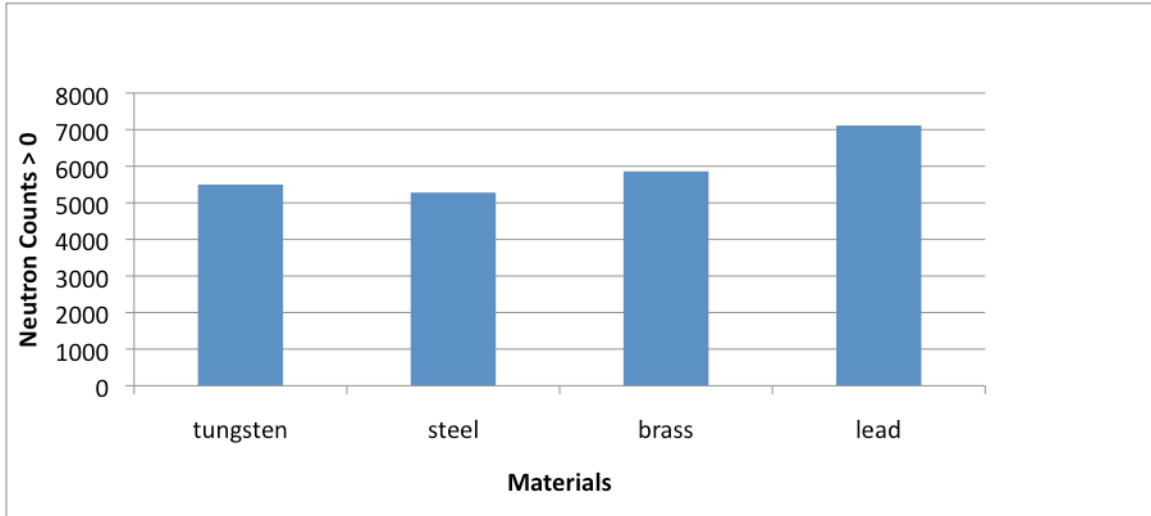


Figure 32. Neutron Production Rate Versus Materials at 0 cm

6.3. Steel Results

Data measured with the IAT detector showed that steel had the least effect of the materials. Steel emitted the least number of neutrons and gave off no multiplicity events of four or more for the measurement time and amount of material used. Steel, having the least physical density of the materials tested, was expected to give the smallest results, as it did. Steel data produced a curve that matched the Poisson distribution, which basically showed that there was no ship effect for this material.

6.4. Tungsten Results

Tungsten had the highest neutron density of the three materials used. Experimental results indicate that it produced the greatest neutron multiplicity counts compared to the other materials. Tungsten proved to follow the pattern of “the higher the neutron density, the higher the multiplicity”. All four materials corresponded with a fit trend line, but deviated from an earlier experiment.

In October 2007, a similar investigation was produced PNNL researchers (Kouzes et al. 2008). In that study, seven different materials were evaluated consisting of Pb, tile, kitty litter, fertilizer, iron, salt, and sand. Their research concluded that the data support the hypothesis that the greater the neutron density of a bulk material, the more likely it is to undergo spallation events from cosmic ray showers, and thus produce ship effect neutron spikes. Less dense materials have correspondingly fewer neutron-producing interactions. This is consistent with the hypothesis that spallation is of less importance for these low neutron density materials, and that their neutron shielding effects outweigh any ship effect impacts. Results from that paper are shown in Figure 33.

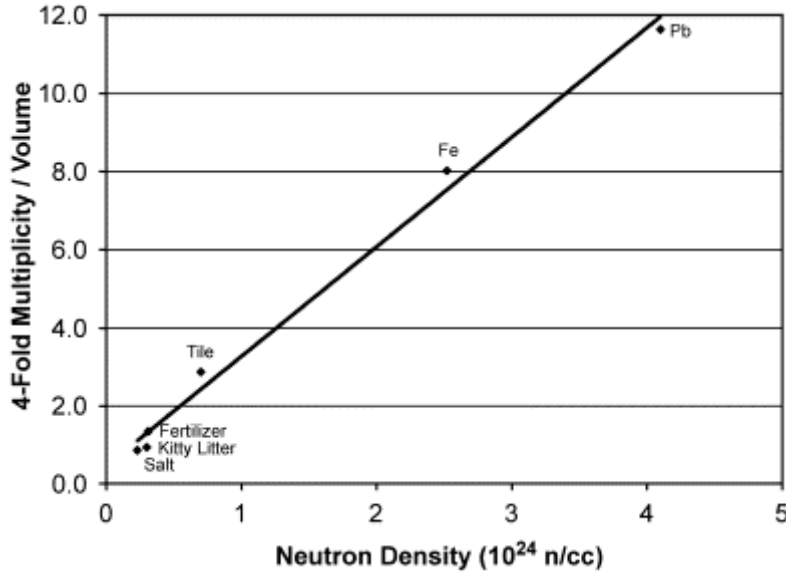


Figure 33. Plot of Neutron Density Versus 4-Fold Multiplicity (Kouzes et al. 2008)

Our research sustain the previous hypothesis of the greater the neutron density of a bulk material compared to the volume of material used, the more likely it is to undergo spallation events from cosmic ray showers, and thus produce ship effect neutron spikes.

Material	neutron density x10 ⁻²⁴	volume m3	Effective Solid Angle	4-fold multiplicity	4-8-fold multiplicity	4-fold mult/ESA/Volume	4-8-fold mult/ESA/Volume
Fe	1.9	0.0151	0.37	0	0	0	0
Brass	2.75	0.0351	0.31	1	3	91.90332	275.71
Pb	4.11	0.0283	0.9	22	32	863.7613	1256.38
W	5.84	0.0032	1.4	6	9	1339.286	2008.929

Table 23. Summary of Multiplicity Results

In Table 19 neutron density for tungsten is the highest of all the other materials, with Pb, brass and steel following in that order. The number of spallation events was expressed as the 4-fold multiplicity and 4 to 8-fold multiplicity. The spallation neutrons were normalized by volume to account for the difference in the quantity of the material samples. The volume specific multiplicity was compared to the neutron density and it was found to increase as a quadratic function, as depicted in Figure 34. The increase in ship effect multiplicity with increasing neutron density is in agreement in general with the previous study, but not in detail when comparing Figures 33 and 34. The reasons for this difference will need to be explored.

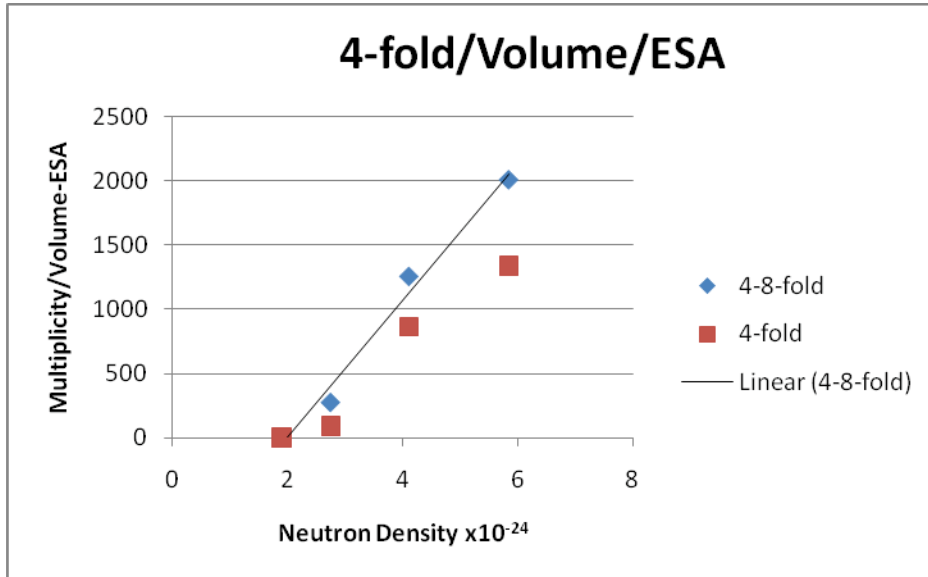


Figure 34. Plot of Multiplicity Versus Neutron Density

7. Conclusions

The main objectives of this research project was to operate, test and characterize an innovatively designed scintillating fiber optic neutron radiation detector manufactured by Innovative American Technology with possible application to the Department of Homeland Security screening for potential radiological and nuclear threats at US borders. One goal of this project was to make measurements of the neutron ship effect for several materials.

The Virginia State University DOE FaST/NSF summer student-faculty team made measurements with the fiber optic radiation detector at PNNL above ground to characterize the ship effect from cosmic neutrons, and underground to characterize the muon contribution.

The neutron detector tested during the present research is based upon a new design: wavelength shifting plastic fibers surrounded by scintillation material and neutron absorber that generate optical scintillations that are collected along the path of the fibers. Spectral analysis is performed with sophisticated computer software to distinguish neutrons from gamma ray induced signals by comparison of the pulse shape and amplitude.

One significant source of variation in the observed neutron background is caused by the ship effect, which gives an enhanced production of spallation neutrons from dense, large masses such as a ship and its cargo.

Measurements of the ship effect above and below ground indicate that less than 10% of the ship effect can be attributed to muons, verifying the assumption that the ship effect arises dominantly from cosmic ray neutron interactions.

This study found an increase in the ship effect with neutron density, but differences with previous work require further research.

The results of this work can be applied to active interrogation techniques and to various non-proliferation monitoring systems, including those deployed worldwide by DOE. For example, this work has the potential to significantly reduce the minimum detectable quantity of plutonium whose detection forms a key element in the SNM detection mission. These methods can be applied to both the currently used ^3He -based neutron detectors and the new generation of alternative neutron detectors.

8. Future Research

Future work will perform similar experimentation to compare results and improve some flaws of this research. One area of improvement is to use materials of the same size and shape, to eliminate the error introduced by correcting for the geometry of the material. The time intervals used for multiplicity event measurements need to be increased to obtain better statistics. These problems will be evaluated to design improved measurements.

9. Acknowledgements

Luke Ericson created the ROOT program and explained a step by step detail into transferring the information from SDC directly to excel without having the trouble to go through PeakEasy. James Borgardt created the code in Mathematica for finding the solid angle using a point source, cube and cylinder. The National Science Foundation provided funding from the FaST Program to support this work. PNNL provided general support, facilities and staff time to aid in this study.

10. Publications

ANSI. 2006. American National Standard Data Format Standard for Radiation Detectors Used for Homeland Security. Technical Report. ANSI N.42.42, American National Standards Institute, Washington, D.C.

Belluscio M, R De Leo, A Pantaleo, and A Vox. 1974. Nuclear Instruments and Methods 114 (1974) 145 – 147

Carchon R, E Van Camp, G Knuyt, R Van De Vyver, J Devos and H Ferdinande. 1975. Nuclear Instruments and Methods 128 (1975) 195 -199

Cook J. 1980. Nuclear Instruments and Methods 178 (1980) 561 – 564

Ely JH, LE Erikson, RT Kouzes, AT Lintereur, ER Siciliano. 2009. “Lithium Loaded Glass Fiber Neutron Detector Tests.” PNNL Technical Report PNNL-18988.

Gotoh, H and H Yagi. 1971. Nuclear Instruments and Methods 96 (1971) 485 – 486

Green MV, RL Aamodt, and GS Johnston. 1974. Nuclear Instruments and Methods 117 (1974) 409 – 412

Guest PG. 1961. The Review of Scientific Instruments Volume 32, Number 2, (1961) 164 -165

- Keller PE and RT Kouzes. 2009. "Influence Of Extraterrestrial Radiation On Radiation Portal Monitors." *IEEE Transactions on Nuclear Science* 56 (3), pp 1575-1583.
- Kernan WJ, RS Detwiler, PC Heimberg. "Ship Effect Measurements Aboard the USNS Regulus January 14-16," April 2003 (September 2003 revised), Remote Sensing Laboratory.
- Knoll GF. 2000. *Radiation Detection and Measurement (2000) 3rd Edition* John Wiley 118 -119
- Kouzes RT, Public protection from nuclear, chemical, and biological terrorism. In: A. Brodsky and R.H. Johnson Jr., Editors, *The 2004 Health Physics Society Summer School, Medical Physics Publishing, Madison, Wisconsin (2004)*, pp. 31–46 (Chapter 3, July 2004).
- Kouzes RT, JH Ely, A Seifert, ER Siciliano, DR Weier, and LK Windsor. 2008. "Cosmic-ray-induced ship-effect neutron measurements and implications for cargo scanning at borders." *NIM-A*, 587:89-100.
- Kouzes RT, JH Ely, PE Keller, RJ McConn, and ER Siciliano. 2008. "Passive Neutron Detection for Interdiction of Nuclear Material at Borders." *NIM A* 584(2-3): 383-400.
- Lintereur AT, JH Ely, RT Kouzes, LE Erikson, DC Stromswold. 2009. "Coated Fiber Neutron Detector Test." PNNL Technical Report PNNL-18919.
- Masket AV. 1957. *Rev. Sci. Instr.* 28, 191 (1957)
- Oblozinsky P and I Ribansky. 1971. *Nuclear Instruments and Methods* 94 (1971) 187 – 188
- Phillips, GW DJ Nagel, T Coffey, A primer of the detection of nuclear and radiological weapons, Center for Technology and National Security Policy National Defense University, 2005, available at (http://ndu.edu/ctnsp/Defense_Tech_Papers.htm)
- Van Ginhoven RM, RT Kouzes, DL Stephen, 2009. "Alternative Neutron Detector Technologies for Homeland Security," Pacific Northwest National Laboratory Report PNNL-18471.
- Vergese K, RP Gardner, and RM Felder. 1972. *Nuclear Instruments and Methods* 101 (1972) 391 – 393
- Wang YF, V Balic, G Gratta, A Fasso, S Roesler and A Ferrari, *Phys. Rev. D* 64 (013012) (2001),p1
- Wielopolski L. 1977. *Nuclear Instruments and Methods* 143 (1977) 577 – 581
- Wielopolski L. 1984. *Nuclear Instruments and Methods in Physics Research* 226 (1984) 436 – 448

11. APPENDIX: Description of Data Analysis Software

The IAT detector uses different software components to process data. The IAT Sensor Data Capture (SDC) software displays and saves the measured neutron data. To extract this data, two programs are used: ROOT (from CERN) and PeakEasy (from LANL). To analyze this data further, Excel is utilized.

11.1. Description of the IAT Sensor Data Capture Software

Sensor Data Capture is IAT software that analyzes data using the command interface and data capture processes. SDC connects to the detector via Ethernet and displays gross counts and spectral images, in the different formats of multichannel, pulse height and width. All collected data can be saved in the IAT proprietary format of .xsp, or as standard N42.42 files (ANSI 2006). Figures 35-37 show each format has its own purpose of collecting data.

Multichannel spectrum illustrates data in line plots of one hundred seconds intervals. These plots indicate the number of multiple neutron events detected. This information can then be saved into folders where it can be accessed at another time by user.

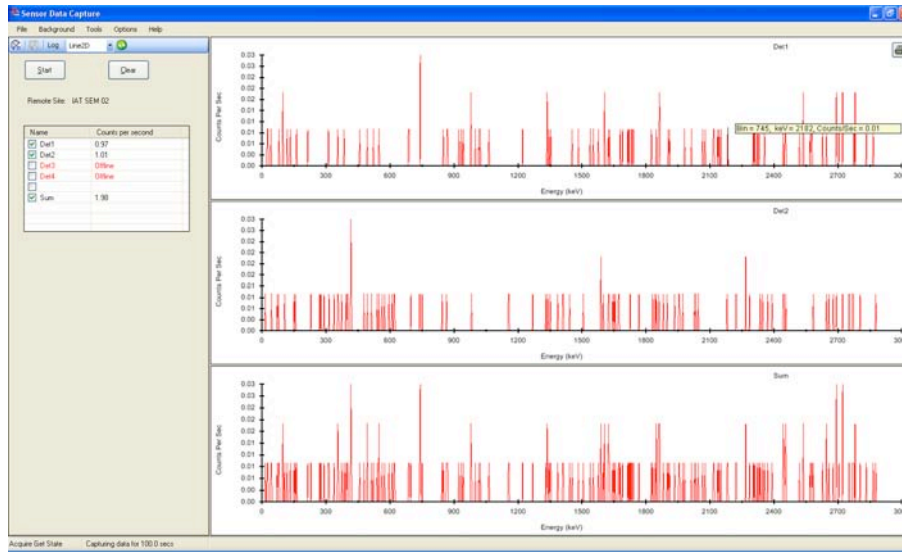


Figure 35. Multichannel View

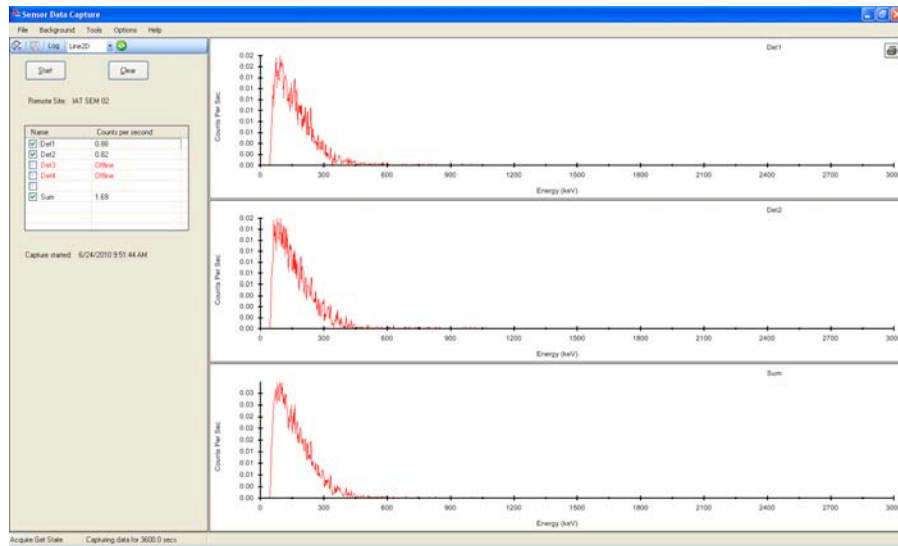


Figure 36. Pulse Height View

The Pulse-height mode shows the number of counts of an electrical pulse if its amplitude falls within specified limits in the form of a histogram spectrum capturing the peaks from the neutron and gamma rays reflected from the source.

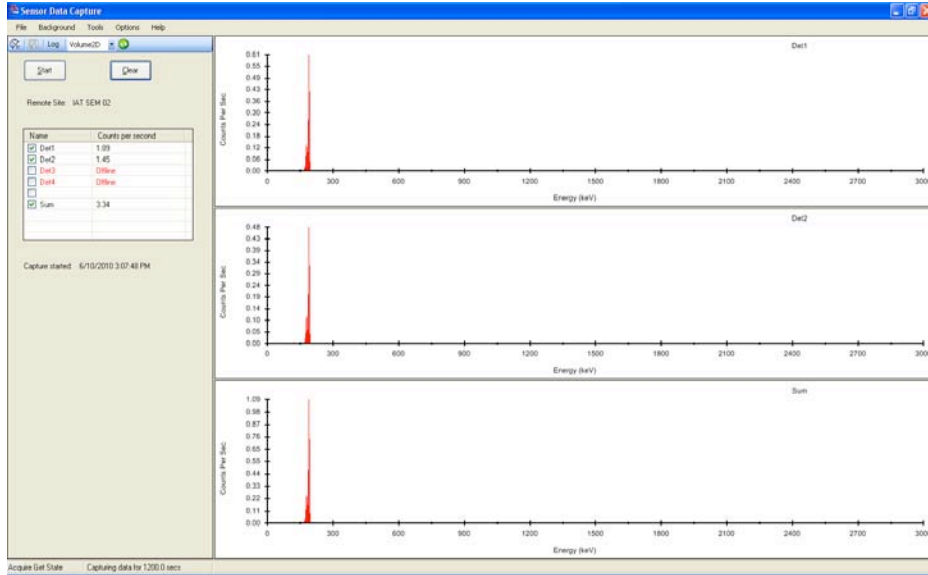


Figure 37. Pulse Width

The Pulse Width mode shows the time interval between the first and last instants at which the instantaneous amplitude reaches a stated fraction of the peak pulse amplitude.

11.2. Operation of the IAT Application SDC

a. Pulse height Mode

1. To start the program click on the SDC icon on the computer desktop
2. Once SDC is open, select file at the top left corner of the page. Then select open remote site from the drop down menu (Figure 38). Pick IAT SEM 02.

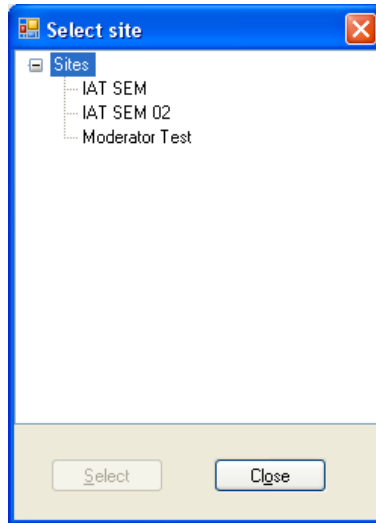


Figure 38. SDC Select Site View

3. Chose detector spectrum the user wants to view by clicking on the box next to the detector name (Det 1, Det 2).

Name	Counts
<input type="checkbox"/> Detector 1	Offline
<input type="checkbox"/> Detector 2	0
<input type="checkbox"/> Detector 3	0
<input type="checkbox"/> Detector 4	0

Figure 39. Detector Selection Menu

4. To change setting to analysis the counts per second in different modes of pulse height Select tools and pick Detector properties from menu.

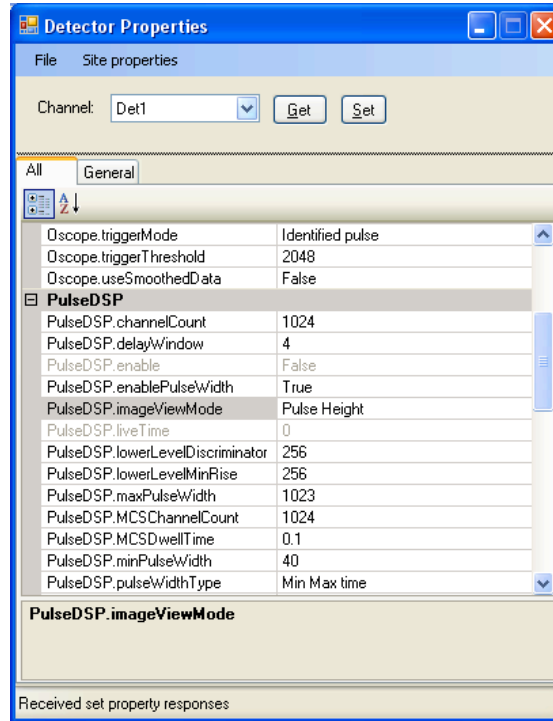


Figure 40. Detector Properties View

- Click down arrow and select detector 1, and then click the get button to the right.

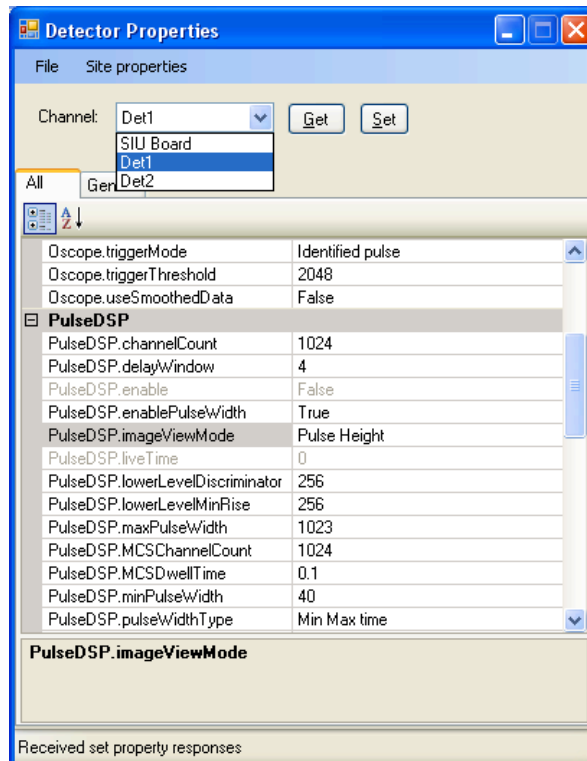
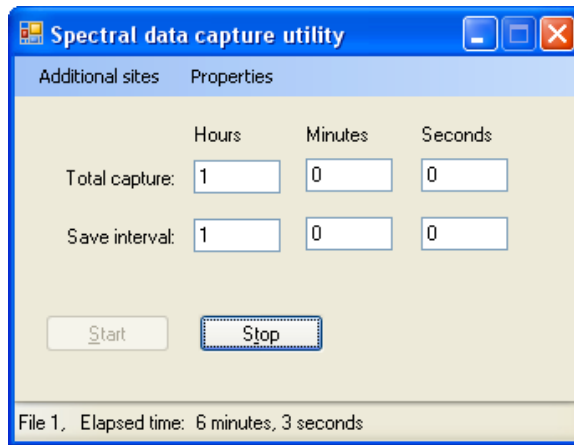


Figure 41. Select Detector View

6. Then scroll down to “PulseDSP.imageViewMode” and click on the down arrow and select a choice.
7. Then go back to the top of the pane and select “set bulk,” this put both detectors in the mode user wants.
8. To set time interval, click on tools, and select Spectral data capture utility (f4) and insert amount of time. For total capture and save interval both must match. Click start to begin data taking.

**Figure 42. Data Capture Utility**

b. Pulse Width Mode

1. Repeat steps above, into step seven and select pulse width instead of pulse height.

c. Multichannel Mode

1. Repeat steps above, from step seven and select multichannel instead of pulse height.
2. In step eight, it's different for the time intervals. In multichannel after every one hundred seconds it saves in a bin. So set the save interval to 100 seconds and insert any amount of time for the total capture.
3. After start you will have to create and select a data folder for the many files produced.

11.3. Description of ROOT Software

The ROOT program provided an easier and more effective way than of transferring saved data from the IAT neutron detector to excel. This program is run through the command prompt and the user has to be precise when loading data or changing directories. Any wrong word or lack of a character would simply result in an error. The most effective way to use this program is to save information in dated folders with the same format (i.e., 6-20-2010, 6-21-2010, etc) all inside of one common folder and directly onto the desktop. Each individual measurement should go into a specific folder to separate the different measurements and distances. This way makes it easier for the user to change directories. With the folder open on the side of the screen as a reference, verify that there is accurate information when changing directories. Make sure to include the “convert.C” file in each specific folder when working with the ROOT program (this routine is used by ROOT in the analysis). The next subsection gives an example set of instructions of how to successfully run the program.

11.4. Application of ROOT software

1. While on desktop click on START which should be located on bottom left of screen.
2. Place mouse over All Programs.
3. Scroll up to Accessories.
4. Now click on command prompt and a black box will appear on the screen.
5. To change directory type the letters “cd “ then followed by the place of the directory whether my documents or desktop (example: cd desktop).

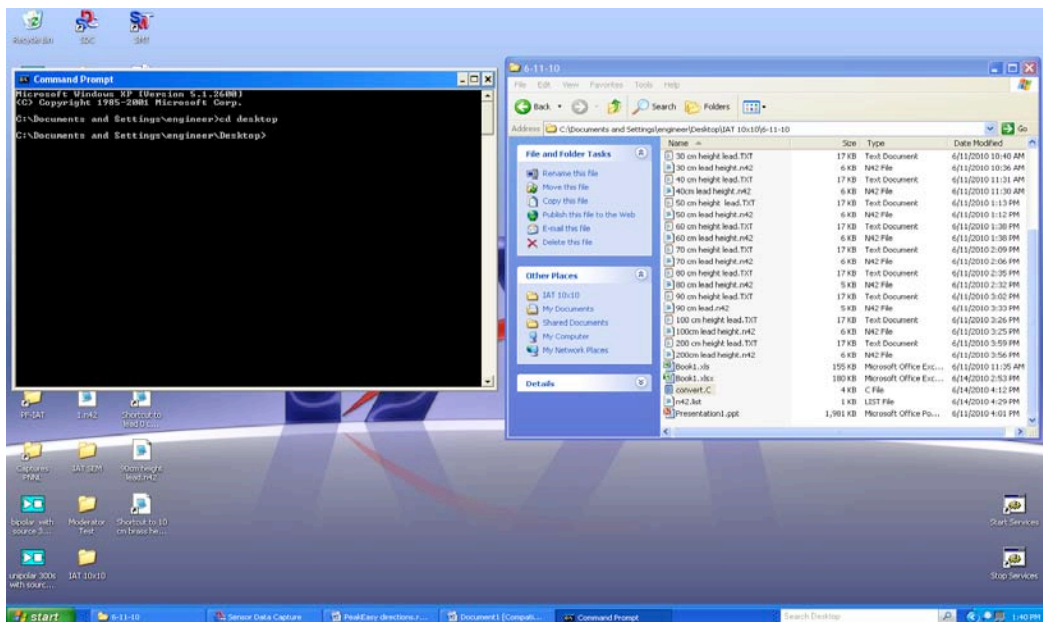


Figure 43. Starting ROOT Software

- Now change directory to common folder (example: cd IAT 10x10)

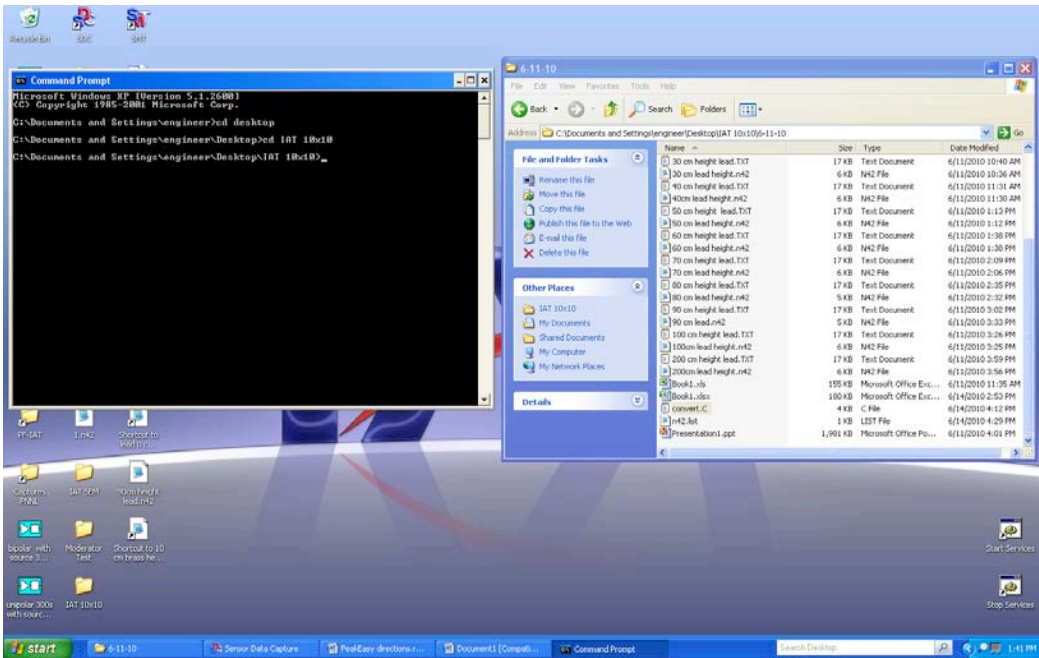


Figure 44. Changing Directory in ROOT

- Change directory to dated folder once common folder is loaded (example: cd 6-20-2010)

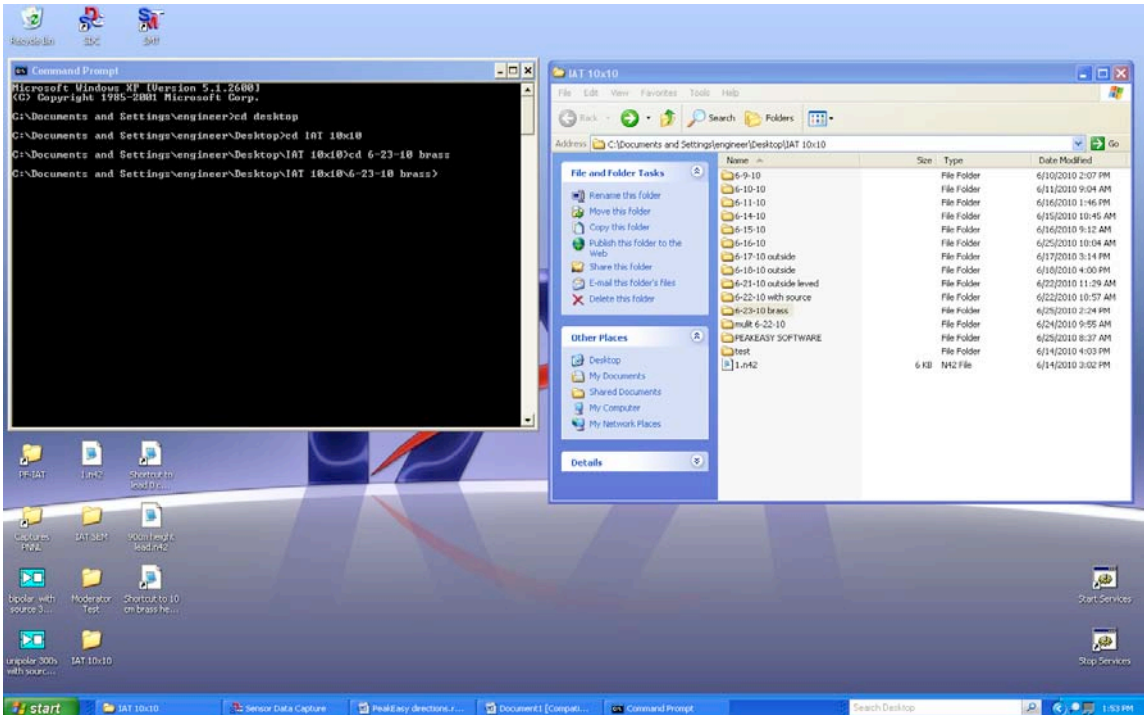


Figure 45. Opening Common Folder in ROOT

- Next change directory to specific folder (example: cd 10 cm)

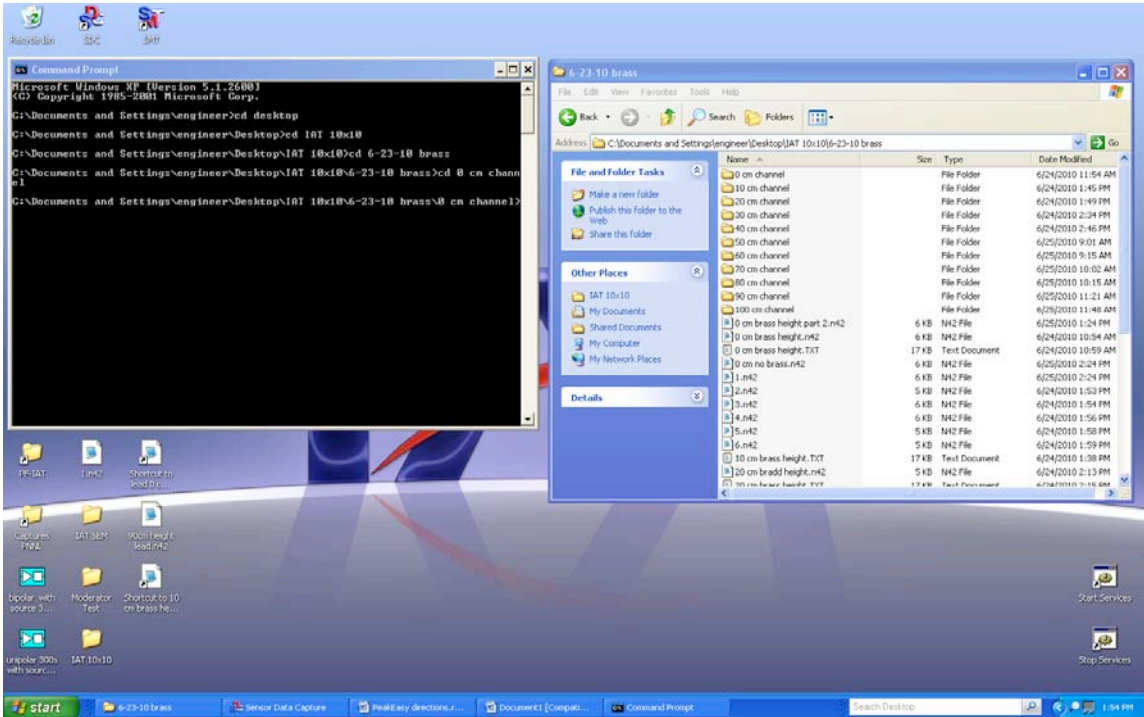
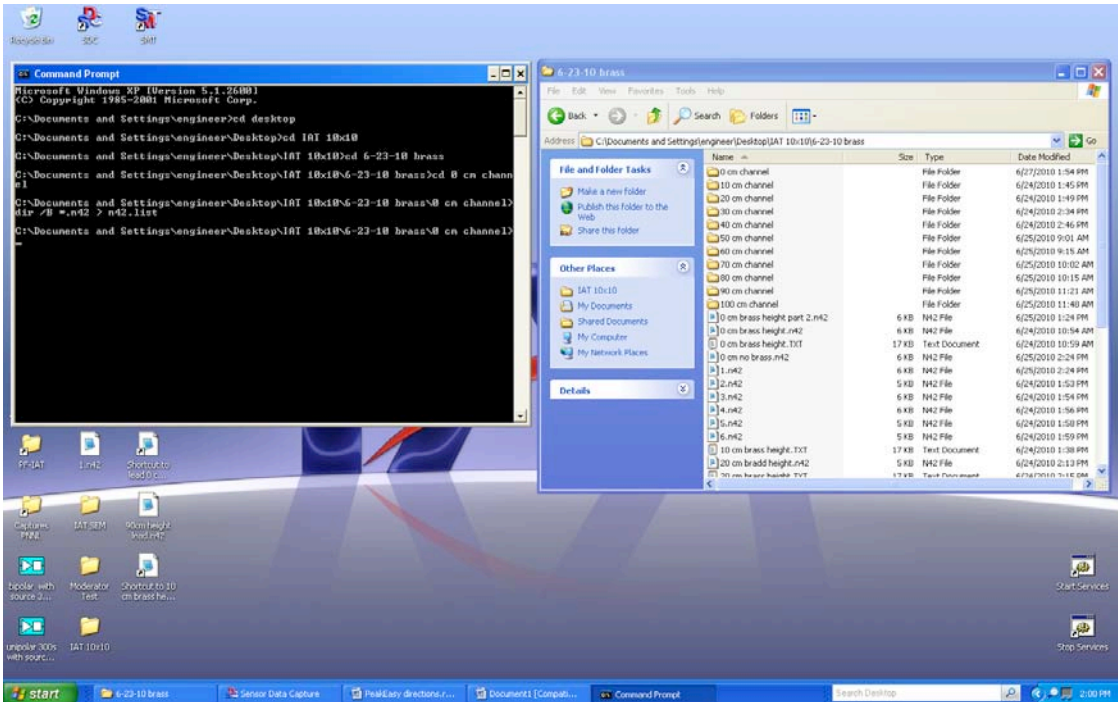


Figure 46. Opening Specific Folder in ROOT

- Now save the directory in the folder (example: dir /B *.n42 > n42.list)



Go back to the command prompt.

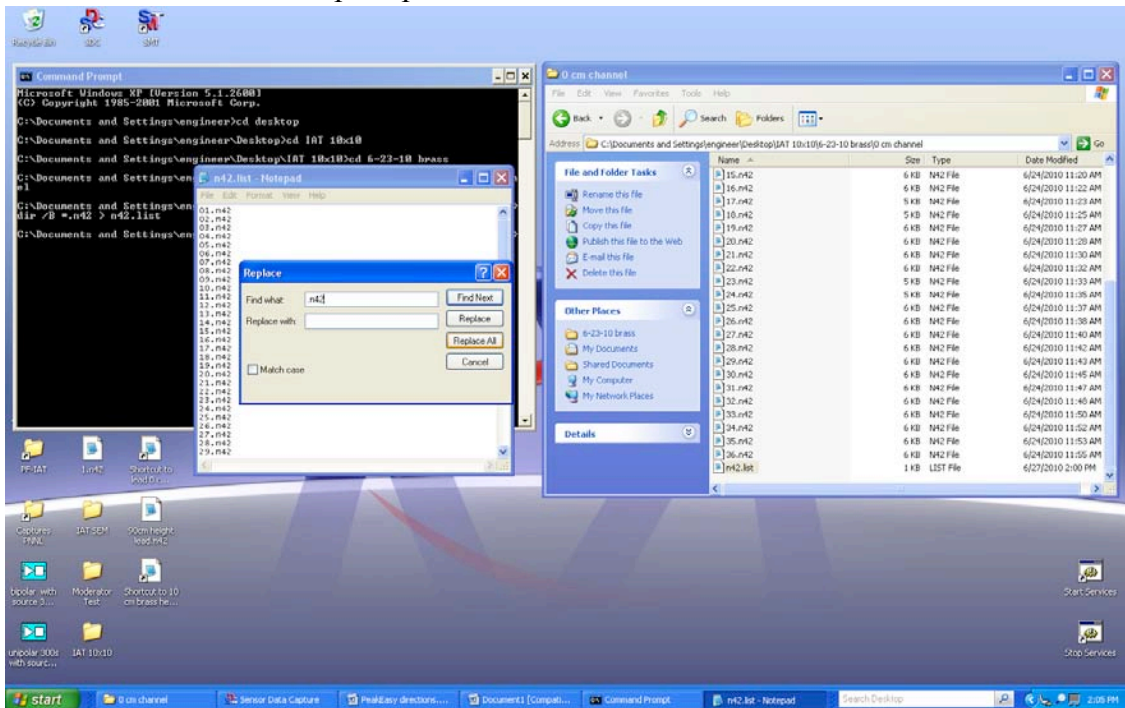


Figure 49. Saving n42.list in ROOT program

12. Once back on command prompt, create a media directory (example: mkdir media)

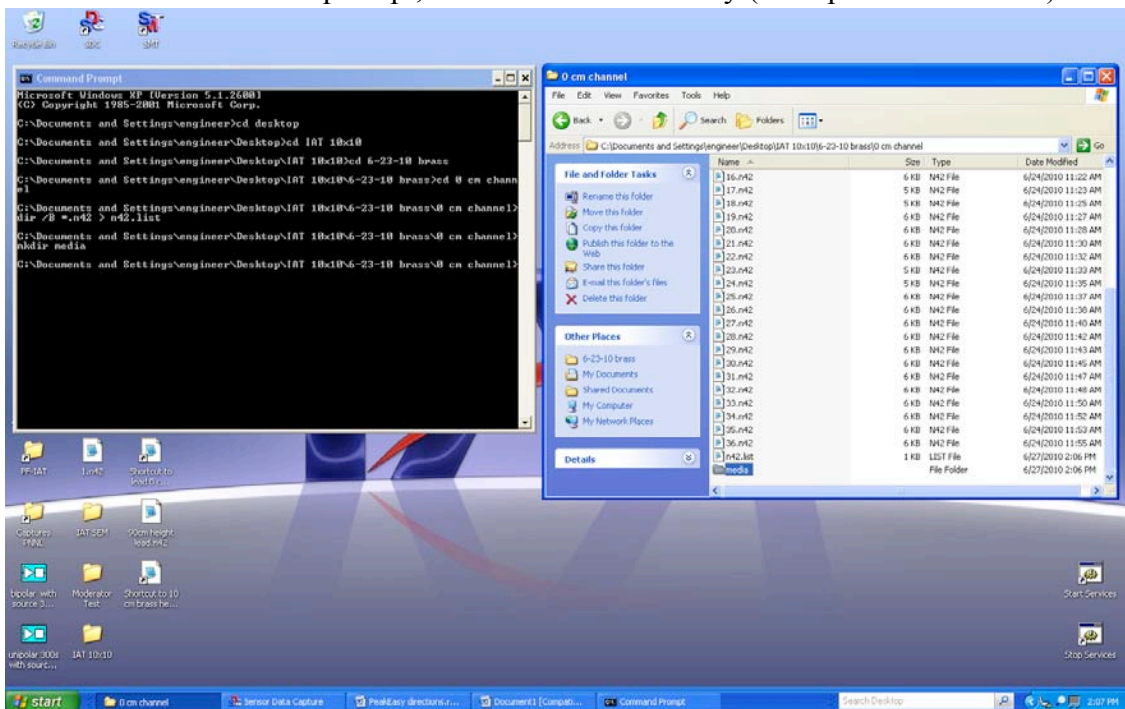


Figure 50. Creating Media Directory in ROOT

13. Now run the program and it will automatically appear in excel (example: root convert.c)

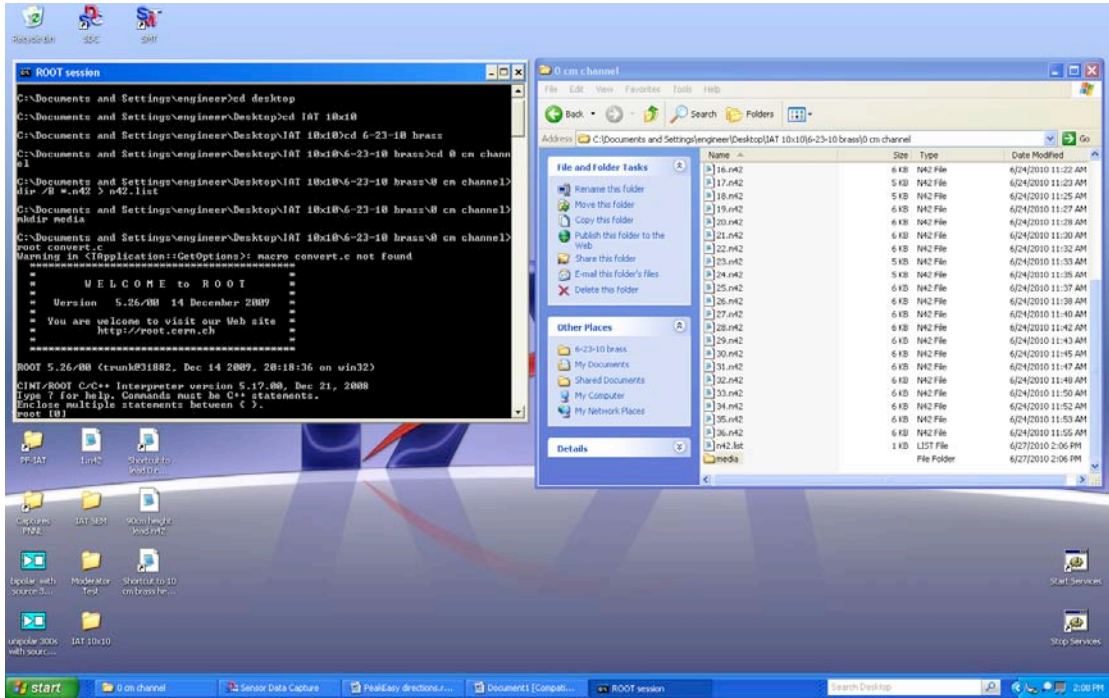


Figure 51. Running ROOT program into Excel

The resulting Excel file (summary.csv) will be located in the media folder. It contains a line for each n42 data file with the multichannel data.

After the specific folder is converted, the user can always go up one directory by typing “cd ..” so it is easier to go to another folder. After moving up one directory, go back and start from step 8 and repeat. If there is any need to escape or exit the directory in ROOT, type the line “q” to end the program. Remember to push Enter after every line is typed.

11.5. Description of PeakEasy

The PeakEasy program is the second step when capturing the image of the spectrum. This step can convert the SDC (sensor data capture) file to a text file which can be easily opened when using Excel.

11.6. Application of PeakEasy

1. Open PEAKEASY SOFTWARE folder from desktop

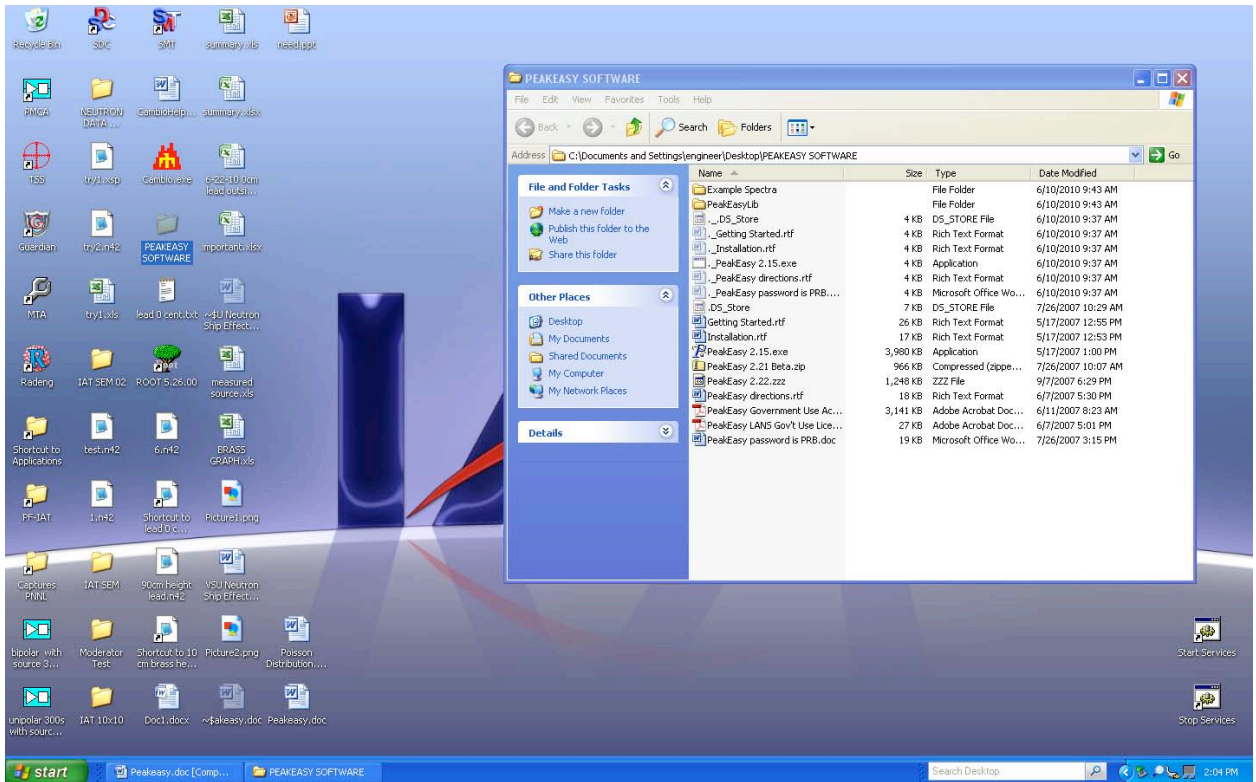


Figure 52. Opening PeakEasy Folder from Desktop

2. Open Application reading PeakEasy 2.15.exe

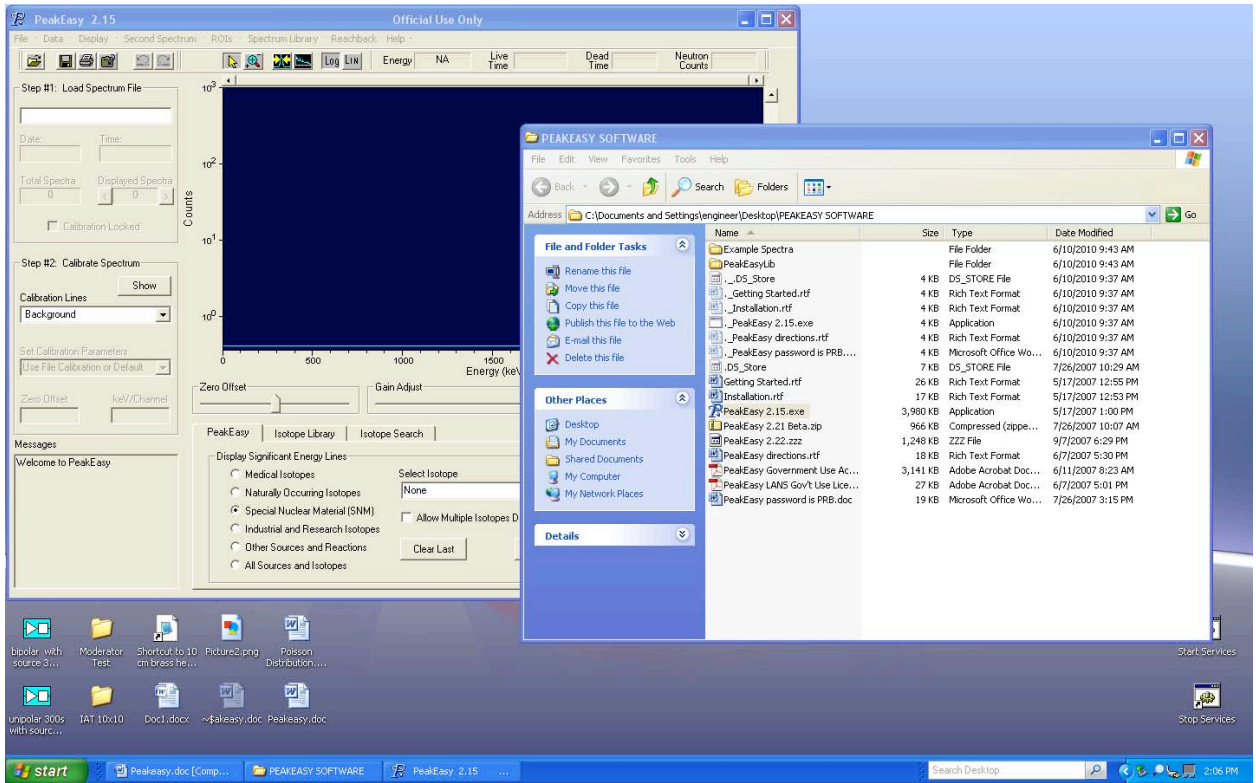


Figure 53. Running PeakEasy Software

3. Click on File and then on Open File/Load Spectra to get to the captured SDC files

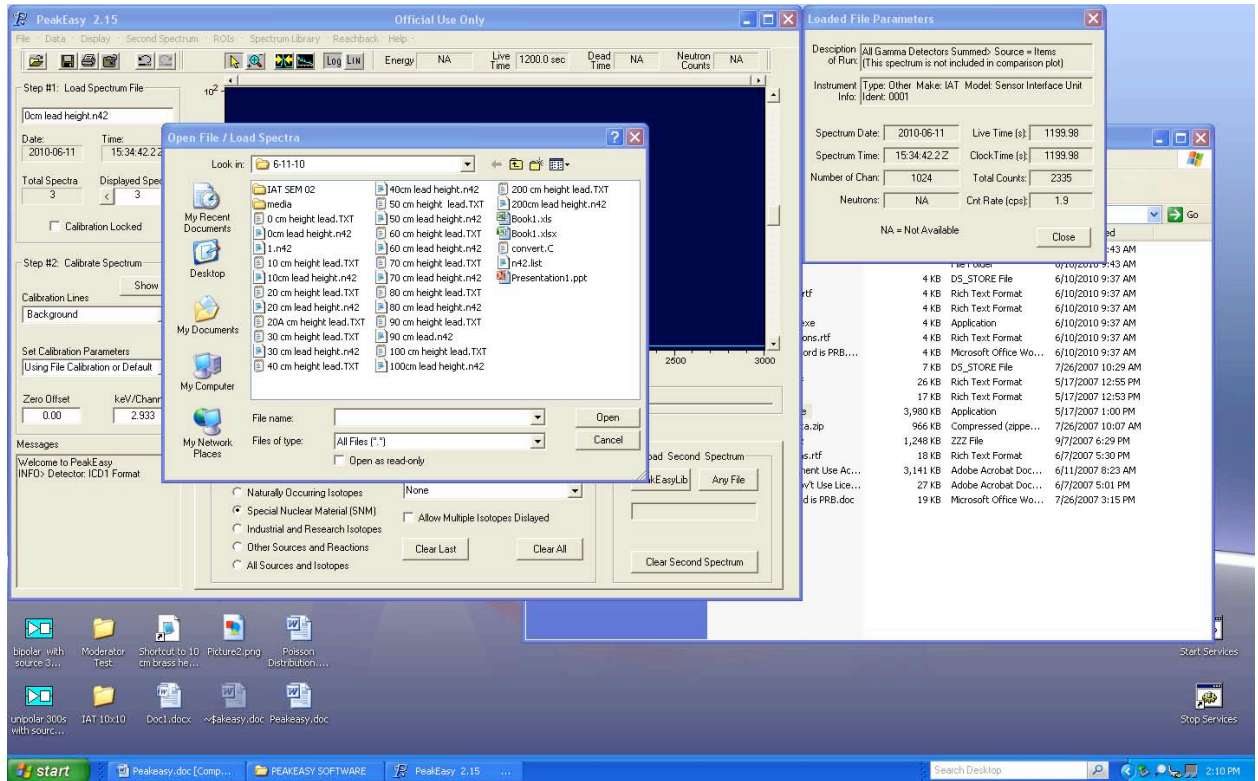


Figure 54. Opening File onto PeakEasy Software

4. Open desired file from SDC

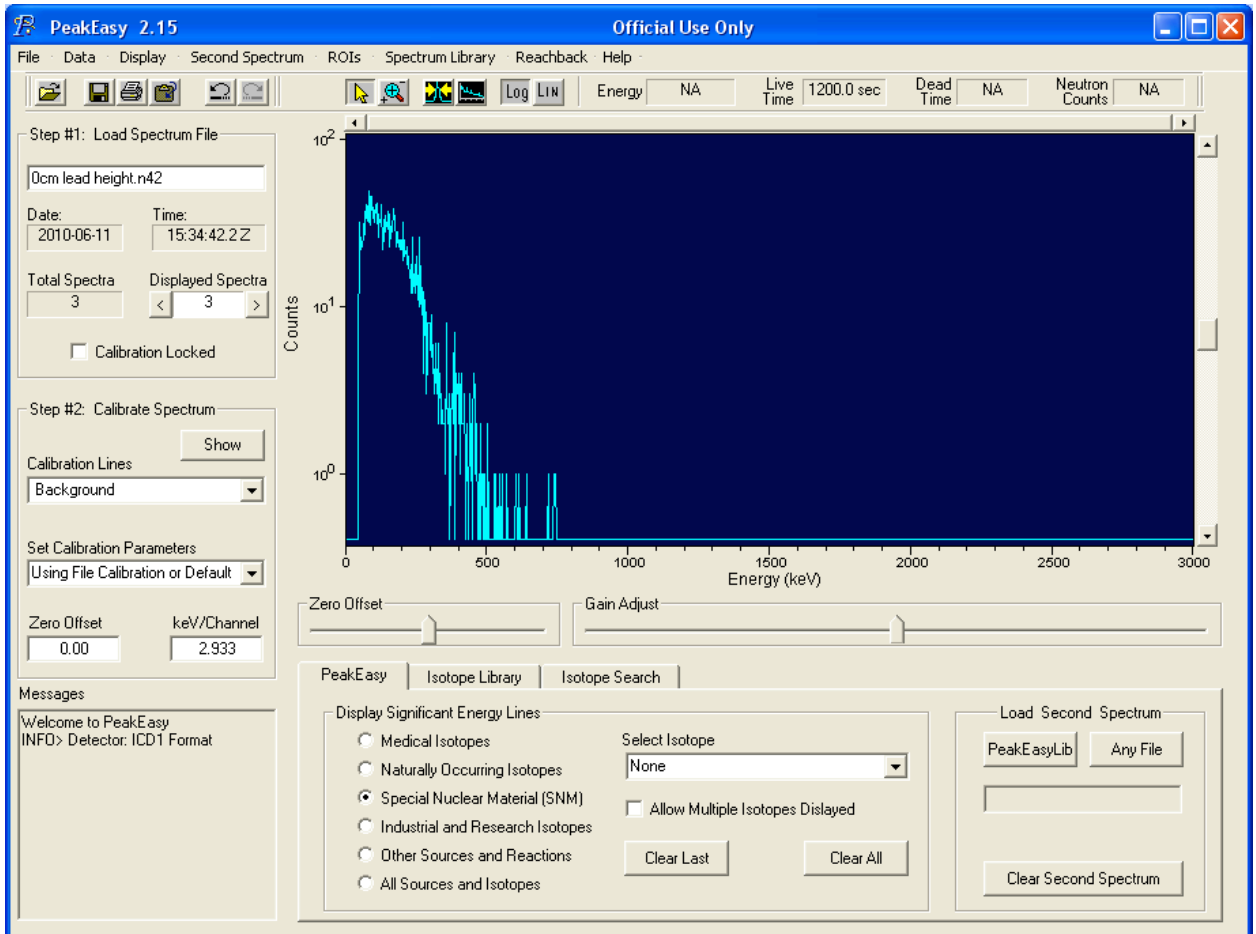


Figure 55. Viewing Spectrum onto PeakEasy

5. Click back on File and save as a Text File

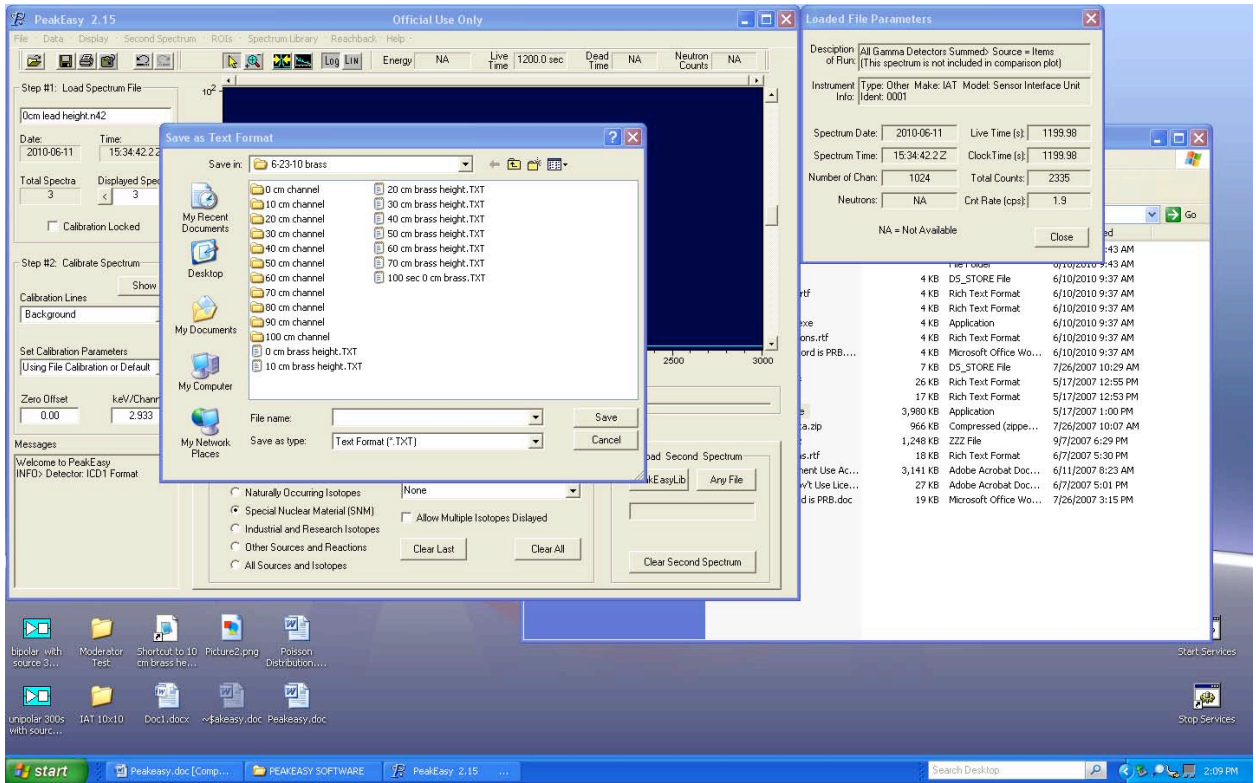


Figure 56. Saving Spectra as Text File on PeakEasy

Now name the file accordingly and save into an easy to reach folder.

It is optional to hold down the buttons Ctrl, Alt and Prnt Scrn to capture the image appearing on the screen so that it can be copied and pasted into a PowerPoint or word document. This would be good if the user was to place each picture into PowerPoint and label it accordingly so that he/she can have a reference for some later time.



Pacific Northwest
NATIONAL LABORATORY

902 Battelle Boulevard
P.O. Box 999
Richland, WA 99352
1-888-375-PNNL (7665)

www.pnl.gov



U.S. DEPARTMENT OF
ENERGY